



AMERICAN UNIVERSITY OF BEIRUT

GROWTH AND CHARACTERIZATION OF PHASE CHANGE  
MATERIALS GROWN BY LASER ABLATION:  
THE CASE OF GERMANIUM TELLURIDE

by  
HADEEL ADNAN SHAHBARY

A thesis  
submitted in partial fulfillment of the requirements  
for the degree of Master of Science  
to the Department of Physics  
of the Faculty of Arts and Sciences  
at the American University of Beirut

Beirut, Lebanon  
February 2019

Beirut, Lebanon  
February 2019

AMERICAN UNIVERSITY OF BEIRUT

GROWTH AND CHARACTERIZATION OF PHASE CHANGE  
MATERIALS GROWN BY LASER ABLATION:  
THE CASE OF GERMANIUM TELLURIDE

by  
HADEEL ADNAN SHAHBARY

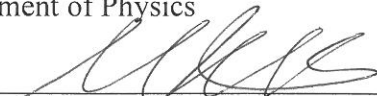
Approved by:



---

Dr. Malek Tabbal, Professor  
Department of Physics

Advisor



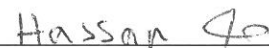
---

Dr. Michel Kazan, Professor  
Department of physics

Member of Committee

---

Dr. Hassan Ghamlouche, Professor  
Department of Physics (LU)



---

Member of Committee

Date of thesis/dissertation defense: [February 6, 2019]



## ACKNOWLEDGMENTS

Foremost I would like to express my appreciation and thanks to my advisors, Professor Malek Tabbal and Professor Hassan Ghamlouche, for encouraging my research and for allowing me to grow my passion as a research scientist. You have been a tremendous mentor for me. Thank you for the continuous support of my master study and research, for your patience, motivation, enthusiasm, and immense knowledge. Your guidance helped me in all the time of research and writing of this thesis. Many thanks also to Dr. Michel Kazan for his advice on both research as well as on my career that have been invaluable. Thank you my committee members, I was truly honored and grateful to work with you.

This work would not have been possible without the financial support of AUB and the opportunities offered in the Central Research Science Laboratory in AUB as well as that in the Lebanese University. Many thanks to all the members of CRSL for their patience and guidance in the experimental work. Your enthusiastic help will leave marks beyond this thesis. I would like to express my gratitude to Dr. Mohamad Roumieh and Mr. Ali Srour, for all the help they provided at the Lebanese CNRS.

I would like to thank all my thesis colleagues, with whom I have shared moments of deep anxiety but also of big excitement. A warm word for my colleague and great friend, Melissa, who always managed to be a major source of support when things would get a bit discouraging. Thank you all for your thoughts, phone calls, and being there whenever I needed a friend.

A special word of thanks goes to my family. Words cannot express how grateful I am to my mother and father along with my sisters and brothers for all of the sacrifices that you've made on my behalf. Your continuous motivation for me was what sustained me thus far. I am especially indebted to my beloved husband, Wissam, for believing in me and being a supportive partner. You are a blessing. My gratitude and love also go to my wonderful baby, Amir, who has been the light of my life for the last two years and who has given me the extra strength and motivation to get things done. Thank you my family for being my unending inspiration.

# AN ABSTRACT OF THE THESIS OF

Hadeel Adnan Shahbary for Master of Science  
Major: Physics

Title: Growth and characterization of phase change materials grown by laser ablation: the case of germanium telluride

Phase change materials (PCM) represent a unique type of materials that can rapidly and reversibly switch between their amorphous and crystalline states. These two phases are characterized by significantly different physico-chemical properties such as electrical conductivity, optical reflectivity, mass density, and thermal conductivity. These differences as well as the repeatability and speed of the switching process make these materials very attractive for data storage and memory devices. Germanium telluride (GeTe) is a chalcogenide PCM which is particularly interesting for device applications because of its large resistivity window (4–5 orders of magnitude between the amorphous and the crystalline state), its the high crystallization speed (~20 ns) and its high crystallization temperature (~180 °C). Typically, thin film deposition techniques such as magnetron sputtering and evaporation are used to growth of GeTe films, but alternatively, Pulsed Laser Deposition can prove to be a method of choice to grow such materials considering its simplicity in depositing high quality materials in a controllable and scalable manner. This thesis deals with PLD of GeTe thin films, and the study of their chemical and physical properties. All deposition runs were performed at room temperature and the effect of experimental growth conditions such as target to substrate distance, background pressure, laser energy, and deposition time on the properties of the films was investigated. The micro-structure of the films were characterized by X-Ray Diffraction (XRD), Rutherford Back-Scattering (RBS) and Scanning Electron Microscopy (SEM) whereas UV-VIS-NIR spectroscopy and temperature dependent resistivity measurements were used to determine their optical and electrical properties. Correlations between deposition conditions and film properties were elucidated and it was found that deposition at an argon background pressure of  $1 \times 10^{-4}$  mbar, a laser energy of 200 mJ and a target to substrate of 6 cm from the substrate, leads to the synthesis of amorphous and stoichiometric GeTe films showing low surface roughness, a sharp transition temperature at about 170 °C and good optical properties with an optical band-gap of 0.77 eV.

# CONTENTS

ACKNOWLEDGEMENTS .....	v
ABSTRACT .....	vi
LIST OF ILLUSTRATIONS .....	x
LIST OF TABLES .....	xii

Chapter

I. INTRODUCTION.....	1
II. THEORETICAL CONCEPTS .....	8
A. Motivation for a New Memory Technology .....	8
B. Principle of Phase Change Materials .....	9
C. Density of States in Amorphous Semiconductors.....	12
D. Electronic Conduction .....	15
1. Extended State Conduction.....	18
2. Hopping Conductivity .....	20
E. Optical Properties .....	21
F. Pulsed Laser Deposition .....	22
1. Fundamentals and General Features of Pulsed Laser Deposition.....	22
2. Advantages and Disadvantages of PLD.....	24

III. EXPERIMENTAL TECHNIQUES .....	26
A. PLD Experimental Setup .....	26
B. Characterization Techniques and Analysis of Thin Films .....	27
1. X-ray Diffraction (XRD) Technique .....	27
2. Scanning Electron Microscopy (SEM) .....	28
3. UV-VIS Spectroscopy .....	30
4. Rutherford Backscattering Spectrometry.....	31
5. Resistance Versus Temperature Measurements .....	33
IV. RESULTS AND ANALYSIS .....	35
A. Effect of Varying the Target to Substrate Distance .....	36
1. SEM Images and Discussion .....	36
2. Film Composition and Thickness Measurements .....	38
3. Optical Properties .....	40
4. Electrical Properties .....	42
B. Effect of Varying the Deposition Pressure.....	46
1. SEM Images and Discussion .....	46
2. Film Composition and Thickness Measurements .....	48
3. Optical Properties .....	51
4. Electrical Properties .....	52
C. Effect Laser Energy.....	54
1. SEM Images and Discussion .....	55
1. Film Composition and Thickness Measurements .....	57
2. Optical Properties .....	59
3. Electrical Properties.....	60
4. Effect of Deposition Time .....	62
a. SEM Images and Discussion.....	62
b. Film Composition and Thickness Measurements .....	63
c. Optical Properties.....	64
d. Electrical Properties .....	65
V. CONCLUSION .....	68



Appendix

A. LIST OF FILMS DEPOSITED IN THIS WORK ..... 70

REFERENCES ..... 72

# ILLUSTRATIONS

Figure	Page
1.1. Tertiary Ge-Sb-Te phase Diagram with Some Chalcogenide Alloys Highlighted..	3
1.2. Crystal Structure of Rhombohedral GeTe .....	4
2.1. Schematic Presentation of the Possible Transformation in the Phase Changes Crystal–Liquid–Amorphous (record) and Amorphous–Crystal (erase) in GeTe .....	10
2.2. Crystallization and Amorphization Processes Along with the Temporal Evolution of Temperature.....	11
2.3. The Density of States Versus Energy .....	14
2.4. Traditional Description of the Density of States in Amorphous Semiconductor ....	15
2.5. Schematic Density of States for Amorphous Semiconductors .....	18
2.6. Hopping Between Localized States .....	20
2.7. A Schematic Representation of the Principle of the PLD .....	23
3.1. Pulsed Laser Deposition (PLD) Setup .....	26
3.2. Bruker AXS D8 Discover X-ray Diffractometer Used.....	28
3.3. Cross Section Representation of the Optical Elements of the SEM .....	29
3.4. The V570 Model UV-VIS Spectroscopy Used.....	30
3.5: Schematic Representation of the Elements in the UV-VIS Setup.....	31
3.6. Layout of a Typical Ion Beam Scattering Setup Including a Tandem Accelerator and Scattering Chamber in Backscattering Configuration .....	33
3.7. The Setup Used to Measure Resistance Versus Temperature Using Two Probe Method.....	34
4.1. XRD Spectra of GeTe Target and GeTe Thin Film (H1) .....	36
4.2. SEM Images of the GeTe Films Deposited at Different Target to Substrate Distance .....	37
4.3. A Typical RBS Spectrum and Simulation for GeTe Thin Film (H1) .....	38

4.4. Variation of the Films' Thickness As a Function of Target to substrate Distance for a Deposition Time of 1:30 Hours and Frequency of 10 Hz.....	40
4.5. Variation of $(\alpha hv)^{1/2}$ Versus Photon Energy (hv) for the GeTe Films Deposited under Different Target to Substrate Distance .....	41
4.6. Resistance of the Deposited GeTe Films Measured with Heating Rates of 5K/min .....	43
4.7. Arrhenius Plots of $\ln(R)$ Versus $1000/T$ for GeTe Films Deposited at Different Target to Substrate Distance .....	44
4.8. SEM Images of the GeTe Films Deposited in Different Deposition Pressure .....	46
4.9. The Variation of Film Thickness As Function of Argon Pressure .....	50
4.10. Variation of $(\alpha hv)^{1/2}$ Versus Photon Energy (hv) for the GeTe Films Deposited Under Different Chamber Pressure.....	51
4.11. Resistance of the Deposited GeTe films at different Argon pressure measured with heating rates of 5 K/min .....	52
4.12. Arrhenius Pots of $\ln(R)$ Versus $1000/T$ for GeTe Films Deposited Under Different Argon Pressure .....	53
4.13. SEM Images of H8, H9, H10, H11 and H12 Samples, the GeTe Films Deposited at Different Laser Energies .....	55
4.14. Variation of the Films' Thickness As a Function of Laser Energy .....	57
4.15. Variation of $(\alpha hv)^{1/2}$ Versus Photon Energy (hv) for the GeTe Films Deposited Under Various Laser Energies .....	59
4.16. Resistance of the Deposited GeTe Films at Different Laser Energies Measured with Heating Rates of 5 K/min .....	60
4.17. Arrhenius Plots of $\ln(R)$ versus $1000/T$ for GeTe films deposited at different laser energies.....	60
4.18. SEM Images of the GeTe Films Are Deposited at Different Time Intervals .....	62
4.19. Variation of $(\alpha hv)^{1/2}$ Versus Photon Energy (hv) for the GeTe Films Deposited Under Various Deposition Intervals .....	64
4.20. Resistance of the Deposited GeTe films at Different Deposition Intervals Measured with Heating Rates of 5 K/min .....	65
4.21. Arrhenius Plots of $\ln(R)$ Versus $1000/T$ for GeTe Films Deposited at Different Deposition Intervals .....	66

## TABLES

Table	Page
2.1. Requirements for Phase Change Media.....	10
4.1. The Atomic Composition and Thickness of Films Deposited at Different Target to Substrate Distance.....	39
4.2. The Optical Band Gap of Films Deposited at Different Target to Substrate Distance .....	42
4.3. The Crystallization Temperature ( $T_c$ ), Electrical Band Gap ( $E_g$ ), and Transition Width of Films Deposited at Different Target to Substrate Distance.....	44
4.4. The Atomic Composition and Thickness of Films Deposited at Different Chamber Pressure.....	48
4.5. The Optical Band Gap of Films Deposited at Different Chamber Pressure .....	52
4.6. The Crystallization Temperature ( $T_c$ ), Electrical Band Gap, and Transition Width of Films Deposited at Various Chamber Pressure .....	53
4.7. The Atomic Composition and Thickness of Films Deposited at Different Laser Energies .....	57
4.8. The Optical Band Gap of Films Deposited at Different Laser Energies .....	59
4.9. The Crystallization Temperature ( $T_c$ ), Electrical Band Gap, and Transition Width of Films Deposited at Various Laser Energies .....	61
4.10. The Atomic Composition and Thickness of Films Deposited at Different Deposition Intervals.....	63
4.11. The Optical Band Gap of films Deposited at Different Deposition Time .....	64
4.12. The Crystallization Temperature ( $T_c$ ), Electrical Band Gap, and Transition Width of Films Deposited at Various Deposition Times.....	66

# CHAPTER 1

## INTRODUCTION

The necessity to store information has always been one of the basic needs of mankind throughout its history. The Cuneiform script, first evidence from 3150 BC, is one of the primal systems of writing. Cuneiform was invented by the Sumerians and is distinguished by its wedge-shaped marks on clay. Almost together with the invention of the cuneiform, the Egyptian hieroglyphs were developed. Hieroglyphics can be pictures of living creatures, objects used in daily life or symbols. The process of storing data through engraving them continued until 1941 in which the first programmable computer –the Zuse Z3 was developed [1]. Since then, electronic and digital data storage has expanded significantly and has replaced physical data storage until the invention of semiconductor memories in the 1970s [2]. In the last few decades, with the explosive development of electronics and computers, this need became an urgency. The past century has seen the development of a variety of different approaches for storing enormous amounts of data, one of the most successful being optical data storage. In optical data storage, information is read from a rotating disc that contains the stored data by detecting the change of reflection of a laser beam focused on the disc. Whereas the first optical storage products only allowed reading of the encoded information, nowadays both recordable and rewriteable storage media have been developed [3]. Initially two different classes of rewriteable optical storage media have been introduced, magneto-optical and phase change media. However, Phase change memory (PCM) is probably the most promising candidate for the next-generation memory. This is based

on the rapid reversible switching between an amorphous and a crystalline state. Both phases are characterized by very different material properties such as electrical conductivity, optical reflectivity, mass density, or thermal conductivity [4]. These differences and the repeatability of the switching give these materials the ability to store information. The material used for memory devices can be organic or inorganic in nature, but typically Phase Change Material refer to inorganic material which may be binary or ternary compositions depending on the application [5].

The theory behind PCM was described in the 1960s, yet the success of optical storage based on phase change materials was only enabled after the discovery of a new class of materials that fulfilled the requirements for this technology [6]. While almost any material including metals, semiconductors, and insulators can exist in an amorphous phase and a crystalline phase, a very small number of materials has the necessary properties that make them useful for data storage technologies. It was found that the GeTe– Sb<sub>2</sub>Te<sub>3</sub> pseudobinary alloys have large optical contrast and could be rapidly and repeatedly switched between the amorphous, low reflectivity and the crystalline, high reflectivity phases using laser pulses. This success triggered a wide interest in PCM technology and an intense research effort has been devoted in the search of materials optimized for this technology [7].

It is common practice to present the stoichiometry featuring the exceptional combination of properties in the so-called “ternary phase-diagram” as depicted in figure 1.1. Most technologically relevant phase-change alloys can be assigned to one of the following families:

1. (GeTe)<sub>x</sub>(Sb<sub>2</sub>Te<sub>3</sub>)<sub>1-x</sub> based alloys: Alloys from the pseudo-binary line between GeTe and Sb<sub>2</sub>Te<sub>3</sub> have been employed in rewritable optical storage media [3,8] Sb<sub>2</sub>Te<sub>3</sub>-

rich compositions, such as  $\text{Ge}_1\text{Sb}_4\text{Te}_7$ , suffer from low crystallization temperatures, which probably preclude the application in memory devices.

2.  $\text{Sb}_2\text{Te}$ -based systems: In such systems, adding Ag, In, and Ge dopants to the base material results in compositions such as  $\text{Ge}_4\text{In}_3\text{Sb}_{67}\text{Te}_{26}$  (abbr. GIST) and  $\text{Ag}_4\text{In}_3\text{Sb}_{67}\text{Te}_{26}$  (abbr. AIST). A stoichiometry close to the latter is employed in rewritable DVDs [3].
3. Ge doped Sb: Compositions from this class include  $\text{Ge}_{15}\text{Sb}_{85}$  and GeSbMnSn alloys [8].
4.  $(\text{GeTe})_y(\text{SnTe})_{1-y}$  based alloys: It was recently demonstrated that  $\text{Ge}_2\text{Sn}_2\text{Te}_4$  ( $y = 1/2$ ) and  $\text{Ge}_3\text{Sn}_2\text{Te}_4$  ( $y = 3/4$ ) display the properties required for the application in phase-change memories. Again, low crystallization temperatures preclude the use of the SnTe-rich alloys and SnTe in particular [9].

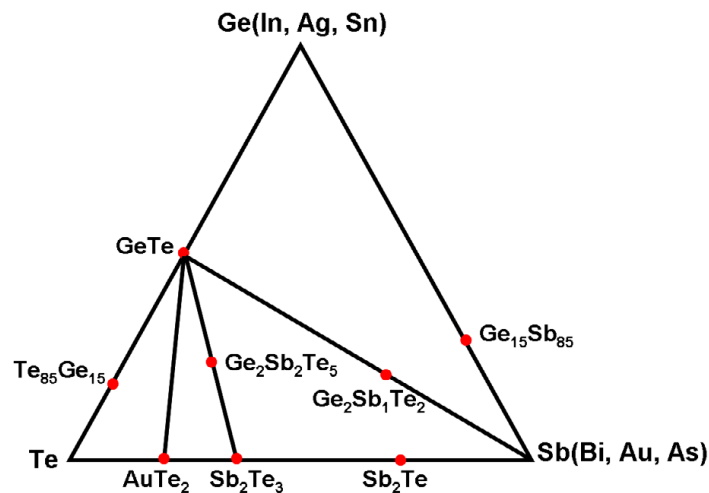


**Figure 1.1. Tertiary Ge-Sb-Te phase Diagram with Some Chalcogenide Alloys Highlighted [8].**

A phase change material should thus have a short crystallization time (nanosecond time scale), a melting point of about 600-800 °C and a high crystallization temperature, typically around 150 to 400 °C [3]. Although much of the existing research

has focused both theoretically and experimentally around  $\text{Ge}_2\text{Sb}_2\text{Te}_5$  (GST), other materials such as the binary compound GeTe are rapidly gaining great attention. GeTe offers a significant improvement of crystallization speed, data retention at high temperature and an excellent contrast in terms of electrical resistivity between the amorphous and crystalline states, when compared to the GST. Non-volatile optical multilevel switching in GeTe phase-change films was identified to be feasible and accurately controllable at a timescale of nanoseconds, which is promising for high speed and high storage density of optical memory devices [10,11,12]. Crystalline GeTe exists in two different forms; the low temperature phase is rhombohedral while the high temperature is rocksalt phase cubic (above  $400^\circ\text{C}$ ). The crystal structures are related, as the low temperature phase can be formed from the rocksalt phase by stretching the lattice and displacing the central atom in the  $\langle 111 \rangle$  direction.

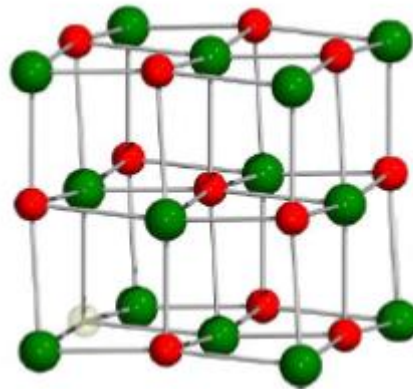


**Figure 1.2. Crystal Structure of Rhombohedral GeTe. The red, green and white spheres symbolize Ge atoms, Te atoms and vacancies, respectively. (From reference [15])**

GeTe has proven to be a material with a very rapid phase change, recrystallizing in just 1 ns. In thin film form, it can be crystallized down to a thickness of 2 nm. With



decreasing film thicknesses, the crystallization temperature rises and the melting point is reduced, leading to better stability and smaller power consumption in devices [11].

In GeTe, the density of the crystalline phase is higher than the one of the amorphous phase, so the volume is reduced after crystallization. Amorphous GeTe has a density of  $5.60\text{g/cm}^3$ , while for the crystalline GeTe it is  $6.06\text{g/cm}^3$ . GeTe thin films have been prepared and characterized by many research groups:

- Howard *et al.* [12] reported results about electrical and optical properties of GeTe films prepared by evaporation. Films were characterized by exponential variation of resistivity with reciprocal temperature. Both optical absorption and photoconductive response have exponential tails toward low photon energies.
- Edwards *et al.* [13] presented a series of DFT calculations of the electronic structure of crystalline germanium telluride and of the intrinsic vacancy and antisite defects in rhombohedral and fcc phases.
- Sarnet *et al.* [11] studied GeTe thin films produced by atomic layer deposition. The films were conformal and stoichiometric and had the required optical and resistivity contrast between amorphous and crystalline phases. Atomic layer deposition is thus concluded by the authors to be an excellent technique for depositing phase change materials.
- Luckas *et al.* [14] investigated the deposition of GeTe films using the sputtering technique. The focus of this study was to investigate the influence of defect states on electronic transport phenomena. It was shown that it exhibits a high electrical threshold switching field and high density of mid gap states
- Khoo *et al.* [15] studied the crystallization of amorphous GeTe films prepared by sputter deposition onto substrates held at different temperatures and deposited at

different sputtering rates. It was observed that the deposition temperature and deposition rate have a significant effect on the nucleation of the crystalline phase, but a negligible effect on its growth. Raman spectral analysis indicates an increase of the number of homopolar Te–Te bonds with decreasing deposition temperature and increasing deposition rate.

As another attractive physical deposition method, pulsed laser deposition (PLD) provides several characteristics including high quality films, options for multi-compositions, quick and accurate control of the deposition process, a simple experimental set up, and the possibility of scaling up the process [16]. Only few studies dealing with the preparation of phase-change films by PLD technique are present. In 2017, a study about GeTe thin films deposited by PLD on BaF<sub>2</sub> (111) substrates was presented by X. Sun [17]. The crystallization temperature for pure GeTe film and its activation energy were investigated and the effect of adding oxygen into GeTe was also considered. The crystallization process was explored for dominant growth temperature regimes related to the amorphous, polycrystalline, and fiber textured states. The optical reflectivity and crystalline quality were both characterized.

Clearly, the potential of PLD as a technique to grow GeTe films has not been fully exploited. The focus of this work is to provide a thorough and systematic investigation of PLD to grow GeTe thin films and characterize their properties in view of their use in data storage systems. The experimental conditions namely target to substrate distance, deposition pressure, laser energy and deposition time were varied. In order to assess the properties of the films as PCMs, the five major physical aspects which include structure transformation, film stoichiometry and thickness, topography, optical properties, and electrical properties have been investigated using X-ray

Diffraction (XRD), Scanning Electron Microscope (SEM), Rutherford Backscattering Spectroscopy( RBS) , UV-Vis spectroscopy, and two probe method, respectively.

Following this introduction, the second chapter provides a background to the theoretical description of the structure of amorphous and crystalline phase of GeTe and to the conduction process, as well as to the optical and electrical properties of the material. The third chapter is devoted to describe the experimental techniques used to prepare the films and characterize them. The results and analysis of the results are presented in the fourth chapter, to finally conclude with chapter 5.

## CHAPTER 2

### THEORETICAL CONCEPTS

#### **A. Motivation for a New Memory Technology**

The ability to store and preserve information is considered an important aspect of the progress of the society. Memory devices can be divided into two groups, volatile and non-volatile memory. In a volatile memory, stored information are lost if the voltage supply is interrupted. Whereas, non-volatile memory can retain the stored data without a power supply connected to it. Technologies like magnetic tapes and magnetic hard disk drives are used to retain the information. These technologies are non-volatile and have random access times of milliseconds to seconds [8]. Information in such systems are stored in the different orientation of the magnetic field of ferromagnetic domains on tapes or discs. The mentioned properties make it perfectly suitable for data backup.

On the other hand, mobile DRAM (dynamic random-access memory) market has been widely used for mobile data storage. Here, light-weight memory is required with large capacity, low power-consumption and short random access times. Therefore, the ideal memory with all these properties is still missing: Either very fast DRAM can be used, which is volatile, thus these memories consume an amount of power even without being operated, or flash memory which is non-volatile. Non-volatility is an important advantage over other electronic memories that are volatile (e.g. DRAM) especially for mobile applications, where battery power is limited and needs to be conserved, yet flash memories are slower than current DRAM.

One potential concept of a unified memory technology is the phase-change random access memory (PCRAM), which is based on the cycling of a phase-change material between its amorphous and crystalline phases. This switching process is nonvolatile in nature, very fast (less than 1 ns) and works even in small volumes (films as thin as 2 nm). Thus, the most fundamental requirements for a unified memory technology are available in these materials and the production of working devices is based on an optimization of the materials' properties [18].

## **B. Principle of Phase Change Materials**

The phase change materials used today are a result of 30 years of ongoing research in the field. They are a rare class of materials in which data is stored through the fast and repeated switching between amorphous and crystalline phase. A large number of phase change materials have been proposed, but only a few materials meet the following requirements: [19]

1. Writability: Enable writing of data.
2. Archiving: Stored information has to be stable.
3. Readability: Easy to read.
4. Erasability: Information should be erasable.
5. Cyclability: Storage medium should allow numerous write/erase cycles.

These data storage requirements can be translated to media requirements (Table 2.1).

**Table 2.1. Requirements for Phase Change Media.**

<b>Storage requirement</b>	<b>Material requirement</b>	<b>Material property</b>
Writability	Glass former	Melting point/layer design, appropriate optical absorption
Archival storage	Stable amorphous phase	High activation energy, high crystallization temperature
Readability	Large signal to noise ratio	High optical contrast
Erasability	Fast re-crystallization	Simple crystalline phase, low viscosity
Cyclability	Stable layer stack	Low stresses, low melting Temperature

In general, atomic arrangement in the crystalline phase is characterized by long-range order, whereas atoms in the liquid state are completely disordered. For the amorphous phase, the arrangement of atoms is short-range orders extending over only a few atomic distance.

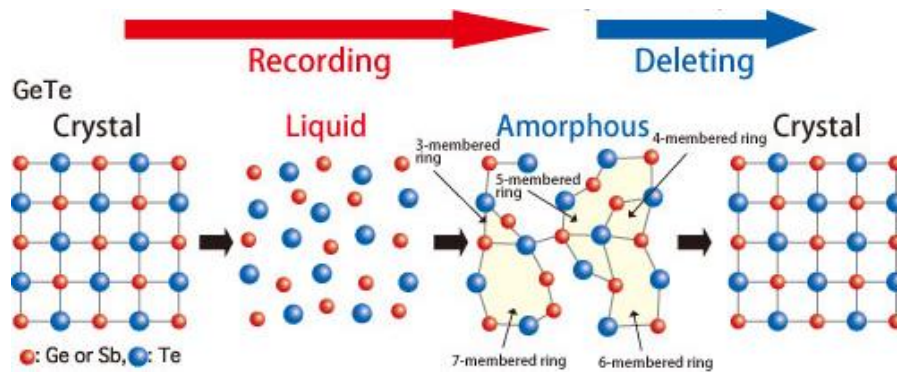


**Figure 2.1. Schematic Presentation of the Possible Transformation in the Phase Changes Crystal–Liquid–Amorphous (record) and Amorphous–Crystal (erase) in GeTe [3].**

Storage operation in PCMs is obtained through the reversible switching of the physical properties between ordered crystalline state and disordered amorphous state. This particular feature of these materials is induced by local heating or cooling either with a precisely controlled laser pulses or electrical pulses.

Crystallization is achieved by heating the amorphous state to intermediate temperature levels above the crystallization temperature while remaining below the melting point, and subsequently subjecting it to a slow cooling. Such a process is called crystallization. On the other hand, amorphization is obtained by heating crystalline materials above melting temperature and quick quenching down it to room temperature. This rapid annealing process generates numerous dislocations or vacancies causing a high resistance [20]. The writing of bits corresponds to the formation of small amorphous regions in the crystalline matrix whereas their re-crystallization leads to the erasure of information.

In phase change materials, it is the change of the microscopic, atomic structure within the volume of the material (not just the surface topology), which contains the information. The low atomic mobility at room temperature allows to preserve the information, whereas the high atomic mobility at elevated temperatures facilitates the writing process.

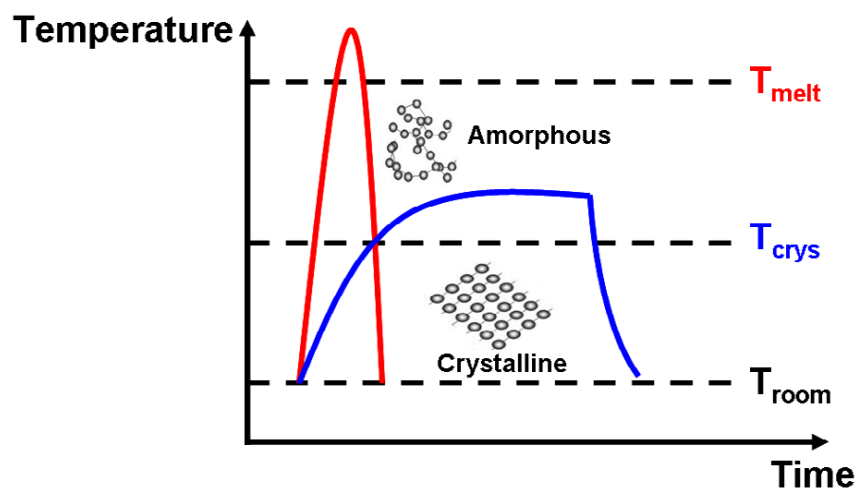


**Figure 2.2. Crystallization and Amorphization Processes Along with the Temporal Evolution of Temperature.**

There are many materials that can be melt-quenched to form an amorphous state, but very few materials also possess a significant difference in optical properties between the amorphous and crystalline state. This optical contrast is due to the difference in atomic arrangement between the two mentioned states, and is found in phase change materials used for optical storage. [21]

In addition, crystallization time commonly considered as the criterion of the switching speed, varies for different PCMs and only those materials with a nanosecond switching regime become suitable for memory devices [20]. These requirements of PCMs are met by the chalcogenide family (Group 6 elements, mainly S, Se, and Te) as well as their derivatives.

### **C. Density of States in Amorphous Semiconductors**

In condensed matter physics, the electronic density of states (DOS) of a system describes the number of states at each electron energy level. It is of a great importance when considering electron transport and optical properties. These states can be occupied or unoccupied and a gap is formed in the density of states characterized by an absence of energy levels. In crystalline solids characterized by translational symmetry, different calculation methods exist to derive the DOS. They are usually based on Bloch electron theory and results are usually displayed in reciprocal space ( $k$  space), inside the first Brillouin zone of the lattice showing symmetry labels. In the electronic DOS of crystalline semiconductors, there is an energy interval referred to as the gap where we cannot find states at any  $k$  value (gaps).

If the maximum energy of occupied and the minimum energy of unoccupied states belong to the same  $k$  than we say that this semiconductor has direct gap. In a



direct band gap, the bottom of the conduction band lies directly above the top of the valence band. On the other hand, in an indirect gap semiconductor the bottom of the conduction band does not lie directly above the top of the valence band. In this case, the electron cannot make a direct transition from the top of the valence band to the bottom of the conduction band. Such a transition can still take place but as a two-step process. The electron absorbs both a photon and a phonon simultaneously [22].

Although crystalline semiconductors have received most attention, yet there is a noticeable effort toward understanding amorphous semiconductors. This is due to the fact that some amorphous semiconductors show unusual switching properties which are important in applications such as memory devices. Moreover, these semiconductors are usually cheaper to manufacture than crystalline ones which leads to a significant reduction in the cost. However, it is hard to treat electron states in a disordered solid due to the pronounced disorder instead of a periodic potential. As a consequence, the Bloch electron theory does not work but band gaps do exist in amorphous materials despite the absence of long range crystalline order.

For a crystalline semiconductor, the bottom of the conduction band (CB) is at  $E_c$  and the top of the valence band (VB) is at  $E_v$ . The interval between these two energies is the energy gap where electron states do not exist in a perfect crystal. Once long-range disorder is introduced into the crystalline state, the effect of this on the energy levels is rather small (only a few percent), because an electron on a particular site interacts most strongly with nearest neighbors. Therefore, the effect of the disorder is to shift the levels up or down by only a small amount through the band. Near the band edge, the effect of the disorder is of great importance since it displaces some levels right into the energy

gap thus creating the band tail. This leads to regions within the band, where charge carriers can be trapped. As shown in figure 2.3, for an amorphous semiconductor of the same substance, the density of states has extended into the gap from both the CB and the VB sides. Each of these states has a “tail” (shaded region in the fig. 2.3) entirely within what was formerly a band gap.

Here we have to make a clear distinction between localized and delocalized electron states. In a localized state, the electron is restricted to movement around only one particular atomic site, while in a delocalized state the electron is extended throughout the solid (existing partly at every atomic site). In case of crystal, all states are delocalized in accordance with the Bloch theorem, while in the case of amorphous solid, both types of states occur simultaneously. The delocalized states are those in the main body of the band just as those in a crystal. On the other hand, the states in the band tail represent localized electrons. [22].

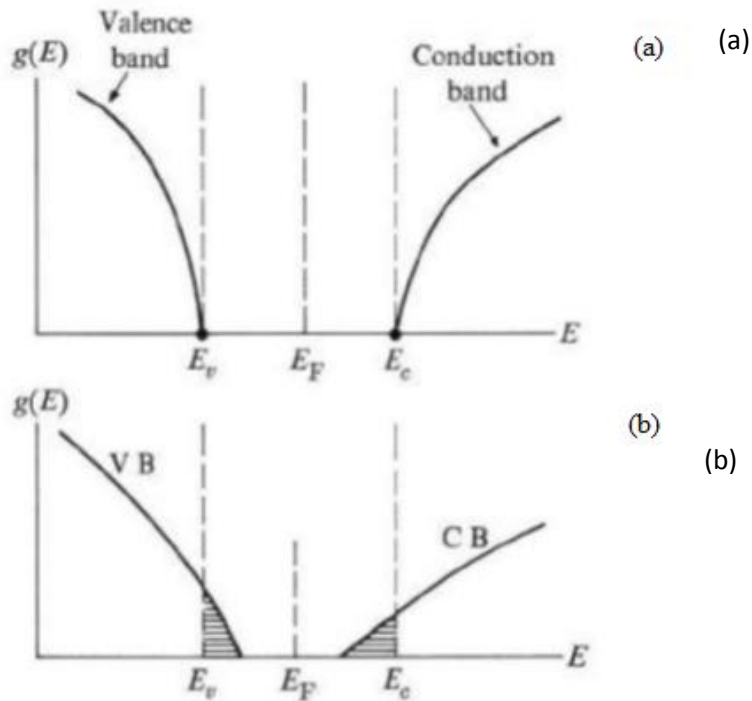


**Figure 2.3. The Density of States Versus Energy. (a) For a crystalline semiconductor; (b) for an amorphous semiconductor. Shaded regions represent band tails introduced by the disorder [22].**

The general description for the electronic density of states of pure amorphous semiconductors is shown in figure 2.4. The band gap usually present in the crystalline semiconductor disappeared. The non-empty gap is referred to as mobility gap (tail), it can be found containing localized electron states which states do not exist in any pure crystalline semiconductors. The rest of states around gap are delocalized and the interface between localized and delocalized states is the mobility edge.

#### D. Electronic Conduction

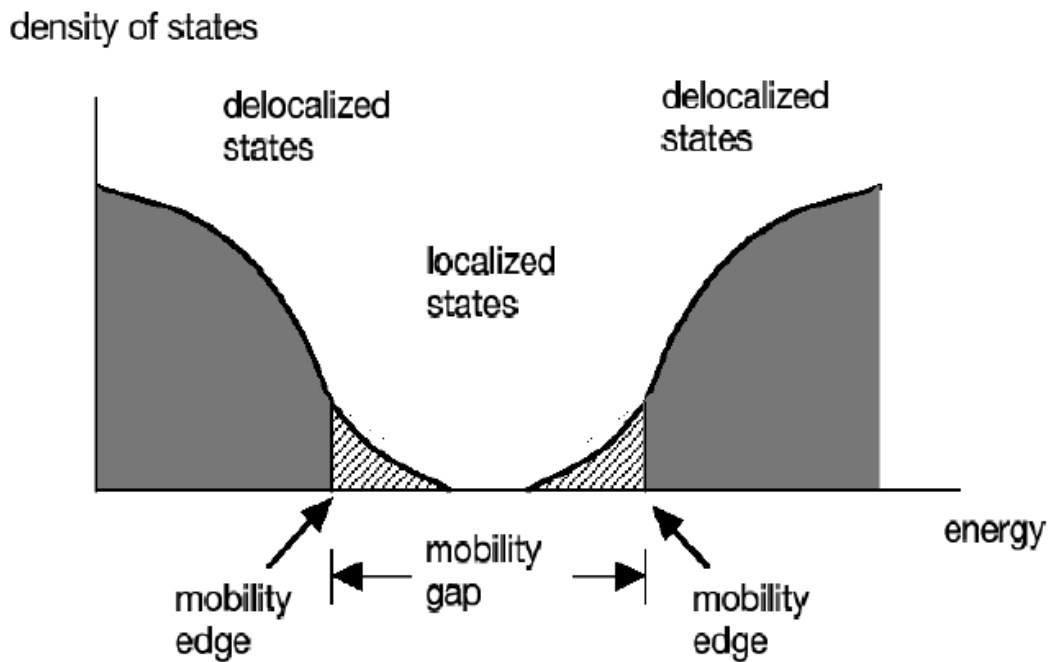


**Figure 2.4. Traditional Description of the Density of States in Amorphous Semiconductor.**

Several models were proposed for the density of states of amorphous semiconductors. All used the same concept of localized states in the band tails which is different than the crystal one with a sharp band. The difference between these models of the amorphous semiconductor lies in the estimate of the extent of this tailing [23].

The DOS function has well-defined energies  $E_v$  and  $E_c$  that separate extended states from localized states as in Figure 2.4. There is a distribution of localized states (tail states) below  $E_c$  and above  $E_v$ . The usual band gap  $E_c - E_v$  is called the mobility gap. The reason is that there is a change in the character of charge transport, and hence in the carrier mobility, in going from extended states above  $E_c$  to localized states below  $E_c$ . The mobility gap is analogous to the band gap in ordered systems but contains the spatially localized states.

Electron transport above  $E_c$  in the conduction band is dominated by scattering from random potential fluctuations arising from the disordered nature of the structure. The electrons are scattered so frequently that their effective mobility is much less than what it is in crystalline.

The concept of delocalization is important in electronic conduction. A delocalized electron moves readily through the solid. Since electrons are distributed through the solid, they need a little push (an electric field for example) to set them a drift, carrying an electric current which is known as metallic conduction. On the other hand, a localized electron is strongly bound to its site and lies deep within the potential barrier. This separates the electron from its neighbors by high potential barrier. Thus to move to another site, the electron has to be energetically excited above the potential barrier. Yet, this barrier is usually about 1 eV such that few electrons are excited at room temperature. This process is known as “hopping” and the thermal excitation process as “activation” [24].

Therefore, electron transport below  $E_c$  requires an electron to jump, or hop, from one localized state to another, aided by thermal vibrations of the lattice, in an analogous way to the diffusion of an interstitial impurity in a crystal. The jump or diffusion of the

impurity is a thermally activated process because it relies on the thermal vibrations of all the crystal atoms to occasionally give the impurity enough energy to make that jump. The electron's mobility associated with this type of hopping motion among localized states is thermally activated, and its value is small. Thus, there is a change in the electron mobility across  $E_c$ , which is called the conduction band mobility edge.

Since the mobility  $\mu$  of a localized electron is essentially zero, we see that for the conduction band for example, there is a sharp drop in the mobility as the energy decreases from the main band to the band tail. The same situation occurs in the valence band. Although a sharp density of states gap is absent, there is a sharp mobility edge in the energy range where  $\mu=0$ . The band is approximately the same as the energy gap in the crystalline solid.

The localized states (frequently called traps) between  $E_v$  and  $E_c$  have a profound effect on the overall electronic properties. The tail localized states are a direct result of the structural disorder that is inherent in noncrystalline solids, variations in the bond angles and length. Various prominent peaks and features in the DOS within the mobility gap have been associated with possible structural defects, such as under- and over-coordinated atoms in the structure, dangling bonds, and dopants. Electrons that drift in the conduction band can fall into localized states and become immobilized (trapped) for a while.

Those marked regions between  $E_c$  and  $E_a$  and between  $E_b$  and  $E_v$  are thought to arise because of the lack of long-range order and are called tail states. In figure 2.5, the states between  $E_a$  and  $E_b$  are defect states which arise from defects in the material and the density of these depends critically on the method used to prepare the amorphous film.

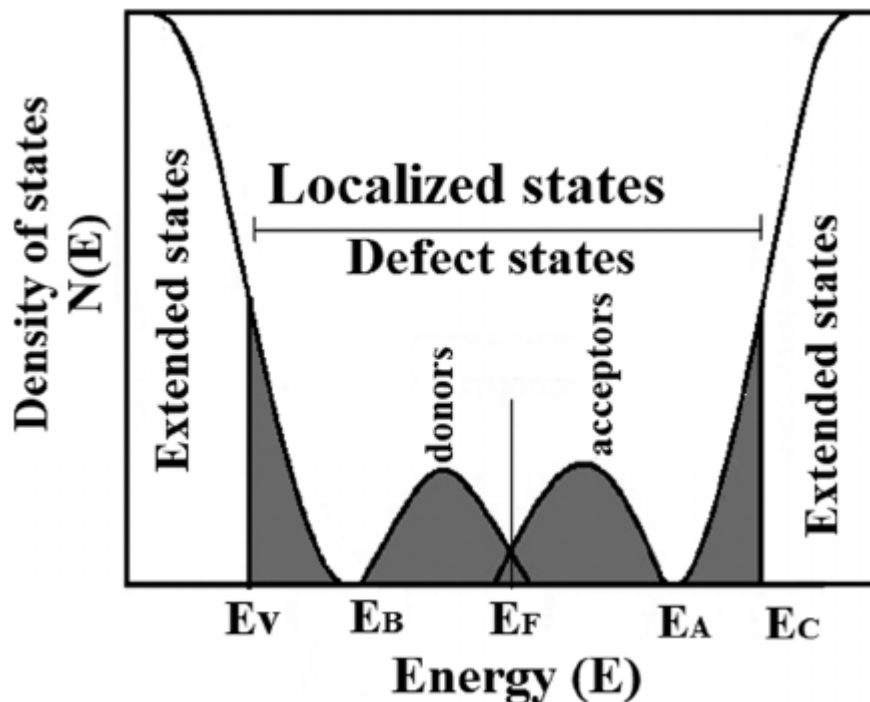


Figure 2.5. Schematic Density of States for Amorphous Semiconductors.

### 1. Extended State Conduction

The conductivity  $\sigma(E)$  depends on  $\mu(E)$ , so we must take a look at the mobility in the various energy ranges.

Consider first the extended states shown in figure 2.5, at energies well into the conduction band where  $E \gg E_C$  and  $E \ll E_V$ , the mobility is similar to that in the crystal. Yet, there is a small probability that carriers occupy these states thus their contribution to  $\sigma$  is not significant.

As the energy decreases approaching  $E_C$  (or  $E_V$ ), the disorder in the lattice increases the scattering where just above  $E_C$  the mean free path of the scattering events decreases from its crystalline value ( of several hundred atomic distances) to a value of

the order of the interatomic spacing [25]. Thus the crystalline theory can no longer be considered because the electron transport may no longer be considered as band motion.

The expression of the conduction in the extended states just above  $E_C$

$$\sigma(E_C) = \sigma_0(E_C) \exp\left[-\frac{(E_C - E_F)}{K_B T}\right] \quad 2.1$$

Where  $\sigma_0$  is the conductivity pre-factor which contains the additional term involving the temperature dependence and  $g(E)$ .

To understand the behavior of the Fermi level in the system, it is useful to start with the situation where  $T = 0$  K. At this temperature, since the donor-like trap has excess electrons, the Fermi level will be between the empty conduction band and the filled trap. When the temperature is above 150 K, the Fermi level is shifted to the middle of the band gap and carrier can be excited across the band gap. In this case the activation energy  $E_A$  is approximately half of the band gap  $E_g$  since it is the difference between the Fermi level and the conduction band. Equation 2.7 can thus be expressed as

$$\sigma = \sigma_0 \exp\left[-\frac{E_g}{2K_B T}\right] \quad 2.2$$

By taking the logarithms of both side of the equation, one has

$$\log \sigma = \log(\sigma_0) - \frac{E_g}{2K_B} \frac{1}{T} \quad 2.3$$

Thus,

$$\log R = \log(\sigma_0) + \frac{E_g}{2K_B} \frac{1}{T} \quad 2.4$$

A plot of  $\log R$  versus  $\frac{1}{T}$  should therefore yield a straight line whose slope,  $\frac{E_g}{2K_B}$ , determines the electrical band gap. [The weak temperature dependence of  $\sigma_0$  is neglected].

## 2. Hopping Conductivity

The states between  $E_C$  and  $E_V$  in figure 2.5 which include tail states and defect states are localized, this leads to the fact that the transport process will not be the same as in the extended states above  $E_C$  or below  $E_V$ . The nature of transport in these states is the hopping process.

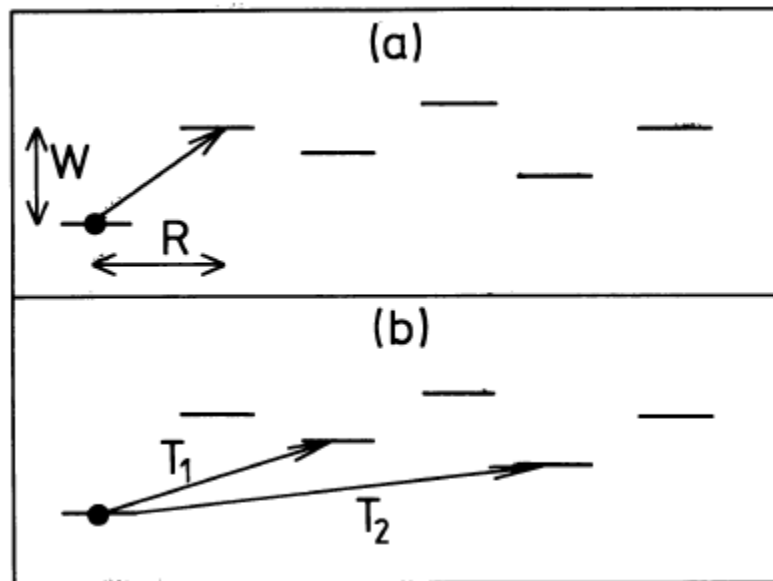


**Figure 2.6. Hopping Between Localized States: (a) nearest neighbor hopping, (b) variable range hopping at lower temperatures,  $T_2 < T_1$**

When this process occurs via states close to  $E_F$ , the conductivity takes the following form which is referred to as  $T^{-1/4}$  behavior [25]

$$\sigma = \sigma_0 \exp\left(-\frac{T_0}{T}\right)^{1/4} \quad 2.5.$$



$\sigma_0$  and  $T_0$  are parameters involving  $g(E_F)$  and the spatial extent  $\alpha^{-1}$  of the electron wavefunction at the Fermi energy.

Therefore, band transport dominates at temperatures above 100 K where the thermal energy is sufficient to excite enough carriers into the bands. Below 100 K and 70 K, hopping transport in the states around 1.3 eV is predominant. At temperatures below 70 K, hopping around the Fermi level takes place [26].

### **E. Optical Properties**

A rewritable CD or DVD comprises a multilayered structure that includes a thin layer of phase change alloy, sandwiched between dielectric layers, deposited on a substrate and capped with a protective layer.

Optical absorption is a standard technique for investigating band structure, and it is therefore of interest to study absorption in semiconductors.

In semiconductors, a number of distinct optical electronic processes take place independently. However, the most important absorption process involves the transition of electrons from the valence band to the conduction band. This process is referred to as *fundamental absorption*.

In fundamental absorption, the electron absorbs a photon (from the incident beam) and jumps from the valence band to the conduction band. For this to occur, the photon energy must be equal to the energy gap  $E_g$  or larger. In the transition process, the total energy and momentum of the electron-photon system must be conserved [22].

As mentioned in section 2.3, when the bottom of the conduction band lies directly above the top of the valence band, the absorption process occurs in the *direct-gap* semiconductors.

In this case, the absorption coefficient has the form [26]

$$\alpha h\nu = \beta(h\nu - E_g)^{\frac{1}{2}} \quad 2.6$$

Where  $\alpha$  is the absorption coefficient,  $h\nu$  is the photon energy,  $\beta$  is a constant involving the properties of the band.

However, calculation of the indirect-gap absorption coefficient was done by Blatt (1968) and the following formula was derived:

$$\alpha h\nu = A(T)(h\nu - E_g)^2 \quad 2.7$$

Where  $A(T)$  is a constant involving the properties of the band and is temperature dependent due to the phonon contribution to the process.

## **E. Pulsed Laser Deposition**

### ***1. Fundamentals and General Features of Pulsed Laser Deposition***

The principle of pulsed laser deposition relies on the use of ultra-short laser pulses, typically tens of nanoseconds that are guided through a beam-line into a high vacuum chamber and are focused by a lens to ablate a solid target.

Due to the high power density of the laser pulses, of the order of  $10^8 \text{ W cm}^{-2}$  or more, the radiation absorbed by the target will be converted not only to electronic excitations, but also to thermal and then mechanical energy which causes energetic

species such as atoms, ions, electrons, molecules, and micron-sized particulates to be ejected from the target in the form of plasma plume. This plasma plume expands and reaches a heated substrate placed above the target whose components participate in the deposition. Deposition is achieved in vacuum or in a chosen background gas in order to reduce contaminants [16].

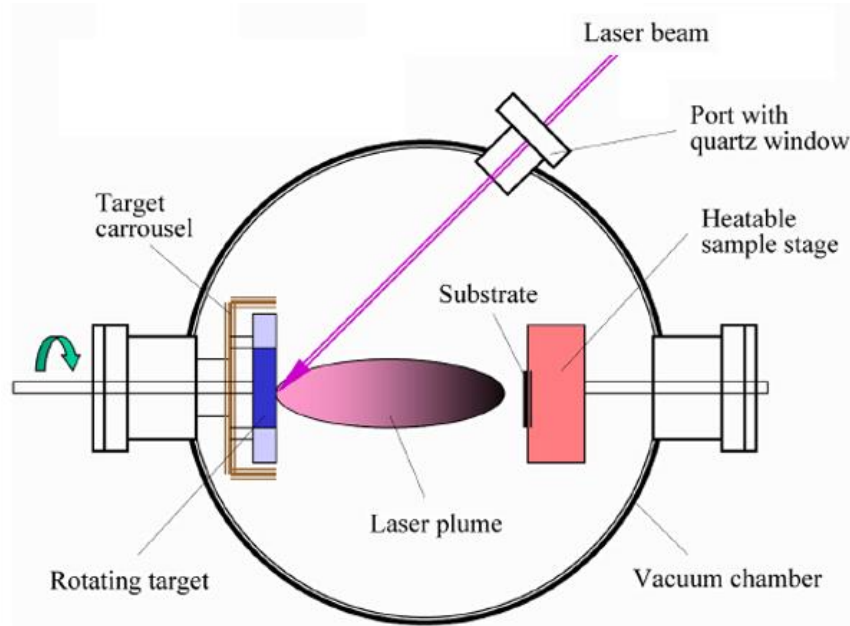


**Figure 2.7. A Schematic Representation of the Principle of the PLD.**

The lasers employed in PLD have ranged from mid infrared radiation such as CO<sub>2</sub> laser (10.6  $\mu\text{m}$ ), to near infrared and visible lasers, like the most often used Nd:YAG laser and its fundamental, second and fourth harmonics (1064 nm, 532 nm and 266 nm respectively), down to the ultraviolet lasers [27]. The latter have been constructed from excimers, unstable molecules, which are formed from a noble gas (xenon Xe, Krypton Kr, argon Ar) in an excited state temporarily bond to a similar atom or a halogen such as fluorine F and chlorine Cl. This molecule then dissociates, within few picoseconds, by stimulated emission emitting a photon in the UV range. Lasers in

which these molecules participate in the lasing action are hence called excimer lasers. Examples are: XeCl (308 nm), KrF (248 nm), ArF (193 nm), F<sub>2</sub>(157 nm)[28].

## ***2. Advantages and Disadvantages of PLD***

The technique of PLD was found to have significant benefits over other film deposition methods, including:

1. The capability for stoichiometric transfer of material from target to substrate, i.e. the exact chemical composition of a complex material can be reproduced in the deposited film.
2. Relatively high deposition rates with film thickness controlled in real time by simply turning the laser on and off.
3. The fact that a laser is used as an external energy source results in an extremely clean process without filaments. Thus deposition can occur in both inert and reactive background gases.
4. The use of a carousel, housing a number of target materials, enables multilayer films to be deposited without the need to break vacuum when changing between materials.

In spite of these significant advantages, industrial uptake of PLD has been slow and to date most applications have been confined to the research environment. There are basically three main reasons for this:

1. The plasma plume created during the laser ablation process is highly forward directed, therefore the thickness of material collected on a substrate is highly non-uniform and the composition can vary across the film.

2. The ablated material contains macroscopic globules of molten material. The arrival of these particulates at the substrate is obviously detrimental to the properties of the film being deposited.
3. The fundamental processes, occurring within the laser-produced plasmas, are not fully understood; thus deposition of novel materials usually involves a period of empirical optimization of deposition parameters.

To a large extent the first two problems have been solved. Films of uniform thickness and composition can be produced by rastering the laser spot across the target surface and / or moving the substrate during deposition. Line-focus laser spots have also been used to obtain large area coverage. The particulate material was initially removed from the plume using a mechanical velocity filter, although recently more elaborate techniques, involving collisions between two plasma plumes or off-axis deposition, have been used to successfully grow particulate-free films. The third problem will be resolved by the development of computer simulations to describe PLD, and will further our understanding of the fundamental physics and chemistry involved in the deposition process.

# CHAPTER 3

## EXPERIMENTAL TECHNIQUES

### A. PLD Experimental Setup

Figure 3.3 shows the PLD workstation setup used in this work. It consists of a high vacuum deposition chamber that can be pumped down to  $10^{-7}$  mbar by a turbomolecular backed by diaphragm pumps. The chamber houses a target manipulator and a substrate holder; the target manipulator can hold up to four different targets and is mounted on rotary drives to allow for its rotation and toggling. The substrate holder is placed on top of the chamber (above the target) with a shutter and a heater that can go up to  $950^{\circ}\text{C}$  as measured by a thermocouple embedded in the substrate holder.

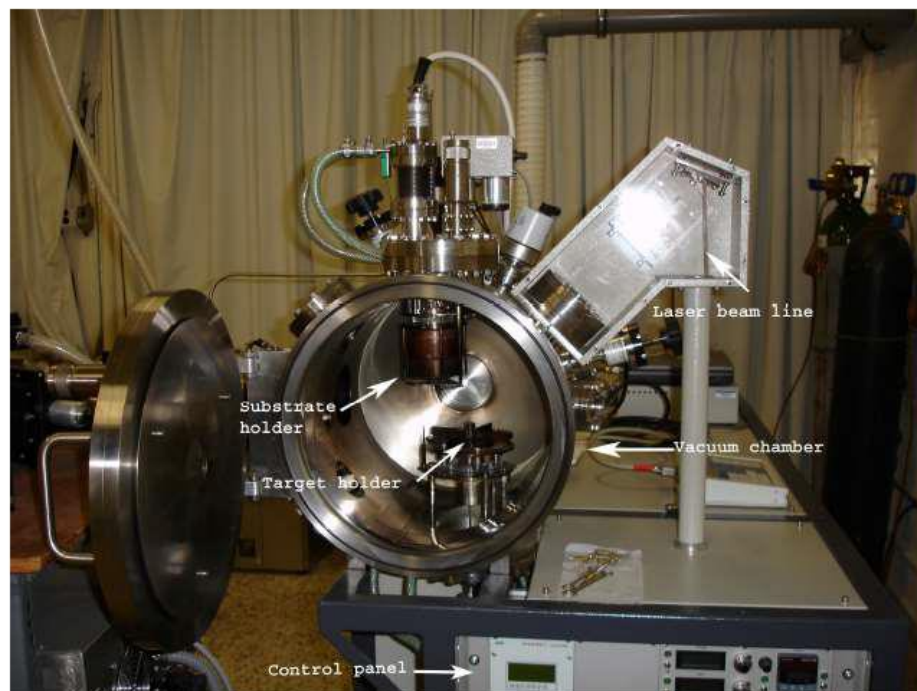


**Figure 3.1. Pulsed Laser Deposition (PLD) Setup.**

The laser used is a KrF excimer laser operating at 248 nm wavelength and 20 ns pulse duration is applied. A beam-line consisting of two mirrors and a lens guides and focuses the laser pulses on the target. The pulse repetition rate is typically set to 10 Hz and the pulse energy is varied between 130 and 350 mJ. GeTe have a high absorption coefficient in the UV range ( $\sim 10^{-6} \text{ cm}^{-1}$ ) [28] and are therefore suitable for the PLD process. The working pressure in the PLD chamber was varied between  $8 \times 10^{-5}$  to  $1 \times 10^{-1}$  mbar during deposition. The substrates are positioned inside the vacuum chamber parallel to the target surface at a target-to-substrate distance of 6 to 10 cm. Both target and substrates are rotated in order to avoid deep ablation of the target and to improve the thickness homogeneity of the films, respectively. In this study, glass substrates have been used.

The substrates were placed in acetone at 60°C for 10 minutes and then for another 10 minutes in methanol at 70°C, after which they were rinsed with double distilled water for 2 minutes and dried with  $N_2$  gas.

## **B. Characterization Techniques and Analysis of Thin Films**

### ***1. X-ray Diffraction (XRD) Technique***

The X-ray measurements were performed using fully automated D8 Discover. In the D8 Discover Bruker diffractometer, the X-ray source consists of a ceramic Siemens tube operating at 40 kV with a current of 40 mA and emitting a Cu  $K_\alpha$  radiation of wavelength  $\lambda=1.5418 \text{ \AA}$ . The diverging x-rays emitted from the x-ray tube are transformed into an intense parallel beam by a Göbel mirror ( Bruker AXS XRD user's manual, 2010), which is free of  $K_\beta$  radiation eliminated by placing a nickel (Ni) filter. A sölle slit placed between the sample and the detector collimates the diffracted beam.

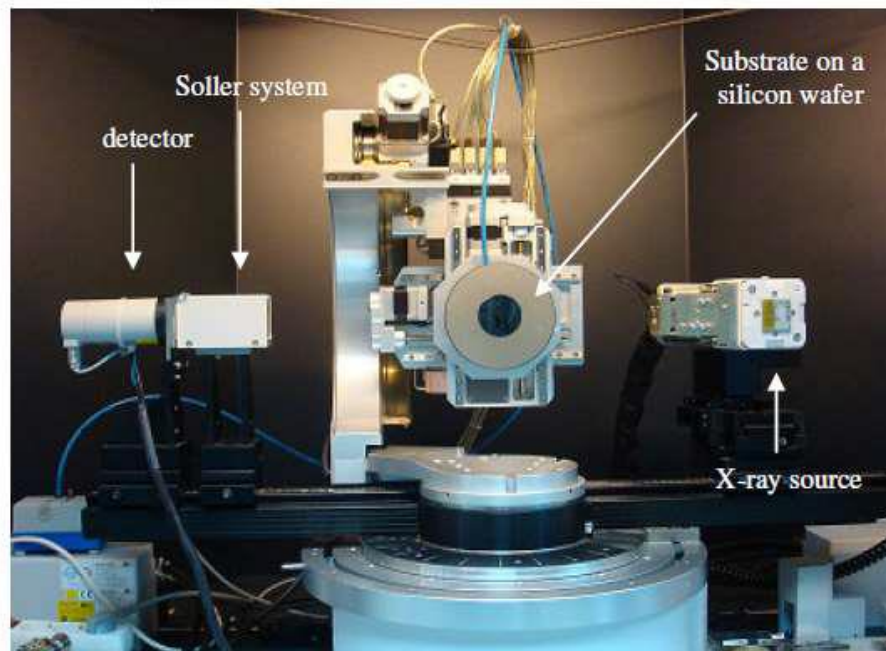


**Figure 3.2. Bruker AXS D8 Discover X-ray Diffractometer Used.**

The parameters chosen for x-ray measurements of all samples are 0.5 s as the time per step,  $0.01^\circ$  as the increment and  $15^\circ$ - $90^\circ$  for the  $2\theta$  range.

## ***2. Scanning Electron Microscopy (SEM)***

Scanning electron microscopy is one of the major electron microscopic methods in which a focused electron beam from an electron gun scans over and across the sample. The electron beam is focused by condenser lenses, beneath which a set of scanning coils deflects the electron beam that is allowed to scan the surface, residing at each point for few microseconds. The deflected electrons called the secondary or backscattered electrons which are in charge of imaging are captured by a detector. The detector converts each into a light flash which produces electrical pulses and which, in



turn, are amplified by a signal amplifier. These amplified signals modulate the brightness of each spot in a two or a three dimensional picture which is displayed on a cathode ray tube (CRT). Hence, every spot on the CRT corresponds to a spot on the surface of the sample. The brightness of a certain area in a SEM image is a measure of the intensity of the secondary electrons detected; the surface areas directly facing the detector will appear bright, while holes and cavities will be pictured as dark areas [29]. The MIRA 3 series scanning electron microscope, which is available in the CRSL, was utilized for imaging the surface of our thin films. It is a family of fully PCcontrolled scanning electron microscopes equipped with a Schottky field emission electron gun designed for high vacuum or variable pressure operations.

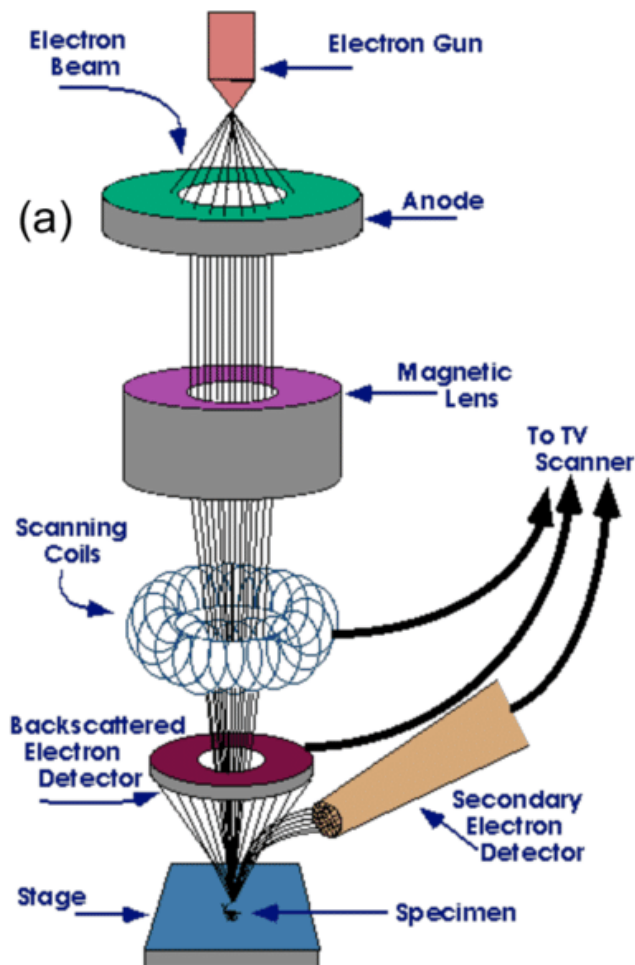


**Figure 3.3. Cross Section Representation of the Optical Elements of the SEM.**

### ***3. UV-VIS Spectroscopy***

The UV-VIS spectroscopy technique is an optical characterization technique that uses ultraviolet, visible and sometimes near infrared (NIR) radiation. This kind of technique has proven to be an efficient technique in determining the band gap of the sample under study.

Our UV-VIS reflectivity measurements were done using the V570 Model UV-VIS spectrometer, available in the CRSL lab, which enables measurements in a broad wavelength range from 200 nm to 2000 nm with an error less than 5%. Light from the spectrophotometer is always polarized by a grating. This spectrometer allows one to measure the absorbance, transmittance, absolute and relative reflectance.



**Figure 3.4. The V570 Model UV-VIS Spectroscopy Used.**

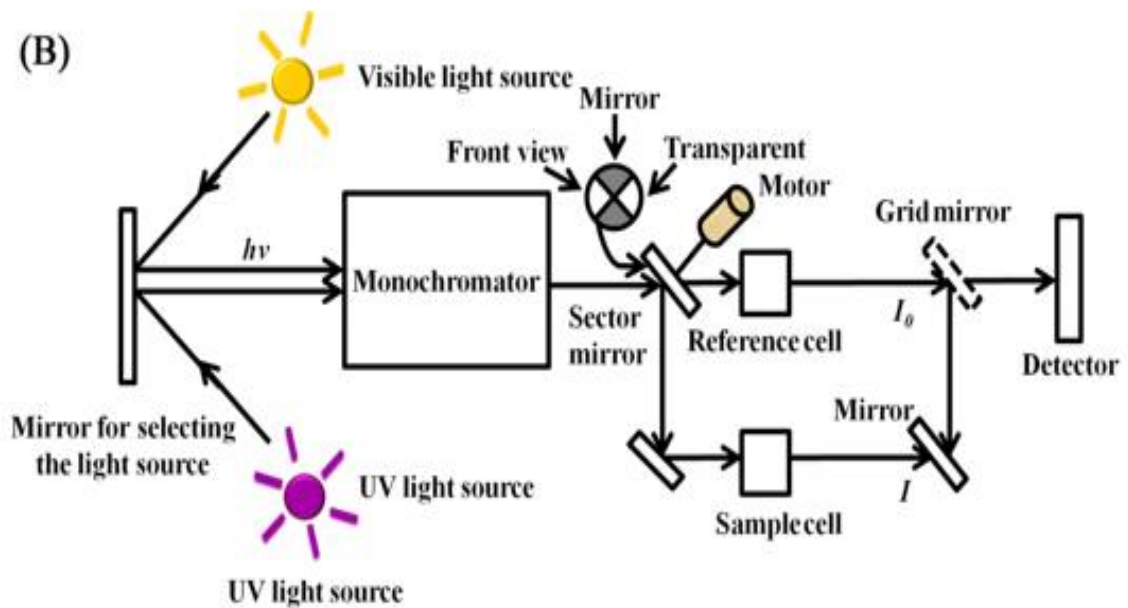


**Figure 3.5. Schematic Representation of the Elements in the UV-VIS Setup.**

Optical absorption and luminescence occur by transition of electrons and holes between electronic states (bands, tail states, gap states). The absorption spectroscopy measures the absorption of radiation, as a function of frequency or wavelength, due to its interaction with a sample. The sample absorbs energy, i.e., photons, from the radiating field and the intensity of the absorption varies as a function of frequency, and this variation is the absorption spectrum.

When an electron absorbs a photon and jumps from the valence band to the conduction band such that the photon energy must be equal to the energy gap.

#### **4. Rutherford Backscattering Spectrometry**

Rutherford Backscattering Spectrometry (RBS) is a widely used nuclear method for the near surface layer analysis of solids. A target is bombarded with ions at an energy in the MeV-range (typically 0.5–4 MeV), and the energy of the backscattered

projectiles is recorded with an energy sensitive detector, typically a solid state detector. RBS allows the quantitative determination of the composition of a material and depth profiling of individual elements. RBS is quantitative without the need for reference samples, nondestructive, has a good depth resolution of the order of several nm, and a very good sensitivity for heavy elements of the order of parts-per-million (ppm). The analyzed depth is typically about 2  $\mu\text{m}$  for incident He-ions and about 20  $\mu\text{m}$  for incident protons. The drawback of RBS is the low sensitivity for light elements, which often requires the combination of other nuclear based methods like nuclear reaction analysis (NRA) or elastic recoil detection analysis (ERDA).

A typical Rutherford backscattering setup consists of a particle accelerator that can deliver beams of low-mass ions in the MeV range. At the Lebanese CNRS, a tandem accelerator is used. This machine produces negative ions that are accelerated towards positive potential. The particles are transported in a vacuum system and at the high voltage terminal electrons are stripped off and the particle charge becomes positive. Then they are repelled by the high positive voltage and increase their energy further. The beam is then analyzed and directed to the target chamber. The beam diameter is about a millimeter at the target.

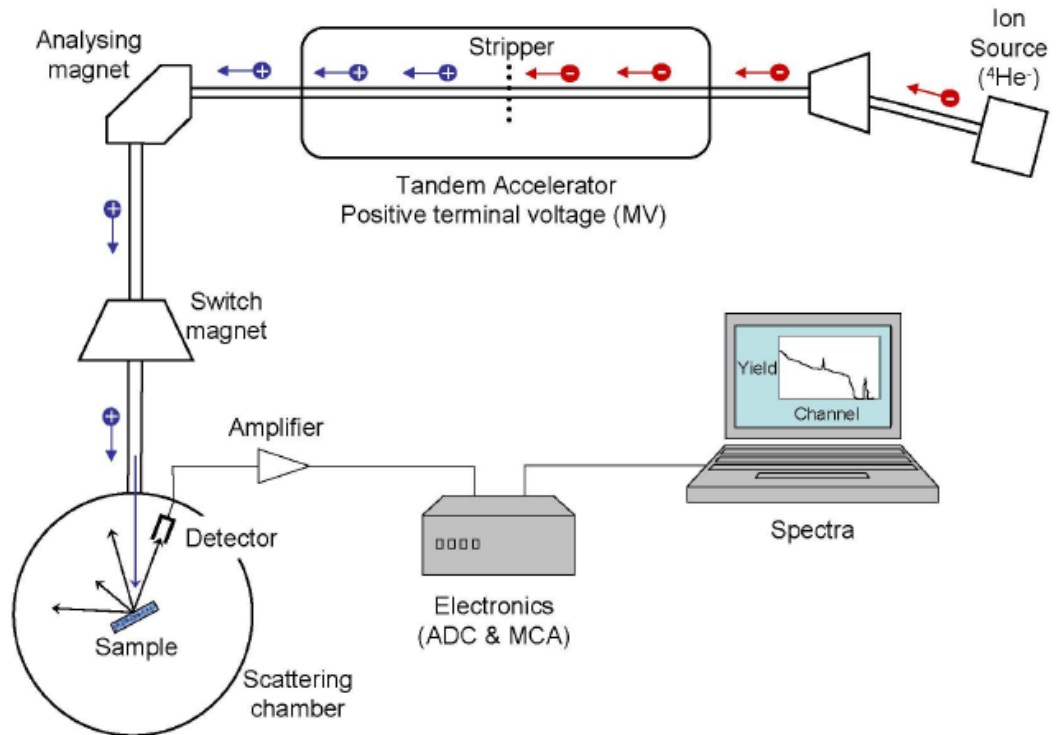


**Figure 3.6. Layout of a Typical Ion Beam Scattering Setup Including a Tandem Accelerator and Scattering Chamber in Backscattering Configuration.**

In our study, RBS technique was used to detect the film composition and its thickness. The GeTe target was bombarded with alpha particles at the energy of 3 MeV and the data was collected using SIMNRA code.

### ***5. Resistance Versus Temperature Measurements***

In order to determine the transition temperature of the thin films and the electrical energy gap, the sheet resistance is measured as a function of temperature using two probe method. The four point probe is usually preferable over a two-point probe. In a four point probe, very little contact and spreading resistance is associated with the voltage probes and hence one can obtain a fairly accurate calculation of the resistivity.

Yet, in our case, two probe methods was used because we want to determine the relative behavior of resistance and not the actual value of resistivity.

The obtained thin film is cut into rectangular pieces. One of the pieces is pasted on an iron block using silver paint. The block is placed on a heating plate, and a thermocouple is inserted inside it. The thermocouple is then connected to a multimeter to read the temperature. Another multimeter is used to read the resistance of the film using two probes method, as shown in figure (3.7). The collected data are analyzed by plotting  $\ln(R)$  versus  $\frac{1000}{T}$ , where the transition temperature and the transition width are determined. The electrical band gap in the amorphous phase is determined from the slope of the curve before transition.

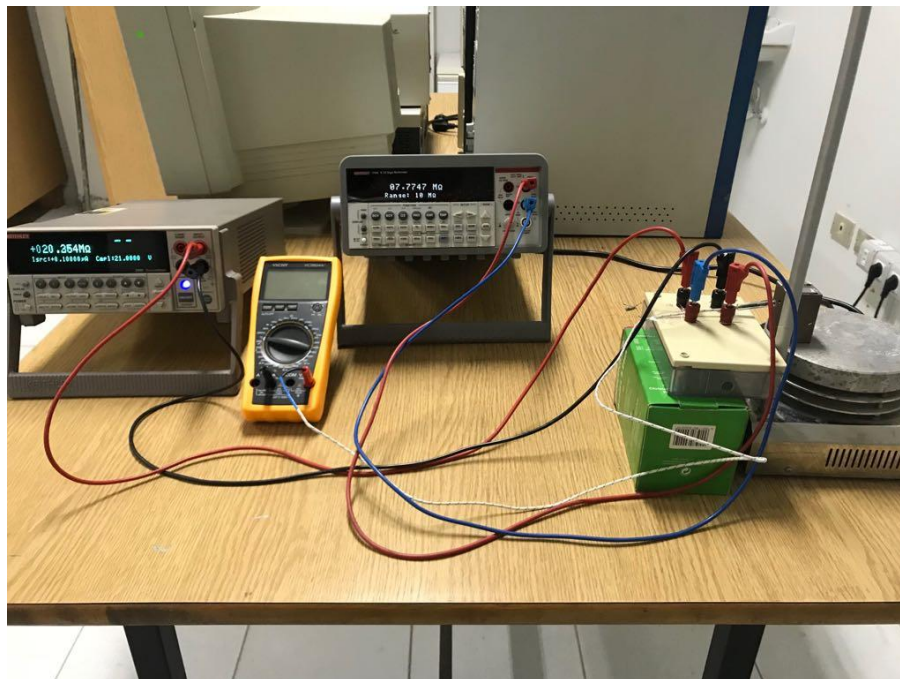


**Figure 3.7. The Setup Used to Measure Resistance Versus Temperature Using Two Probe Method.**

## CHAPTER 4

### RESULTS AND ANALYSIS

In this chapter, we present the experimental results obtained in this thesis. In particular, we show the effect of several experimental parameters (target-substrate distance, chamber pressure, laser energy) on the structural, morphological, optical and electrical properties of the films using the characterization techniques described in chapter 3.

One common feature that is observed for all grown films is that they are amorphous. This was deduced from their XRD pattern. As an example, Figure 4.1 shows the XRD pattern of the GeTe target as well as the film deposited at a 6 cm target to substrate distance, laser energy 200mJ, argon pressure  $10^{-4}$  mbar and 1:30 hours of deposition. The XRD pattern of the target shows diffraction peaks at the angles  $26.1^\circ$ ,  $29.9^\circ$ ,  $42.4^\circ$ , and  $43.3^\circ$  whereas the XRD pattern of all our deposited films show a very broad peak in the  $2\theta$  range between  $25^\circ$  and  $30^\circ$ , indicating an amorphous state of the film.

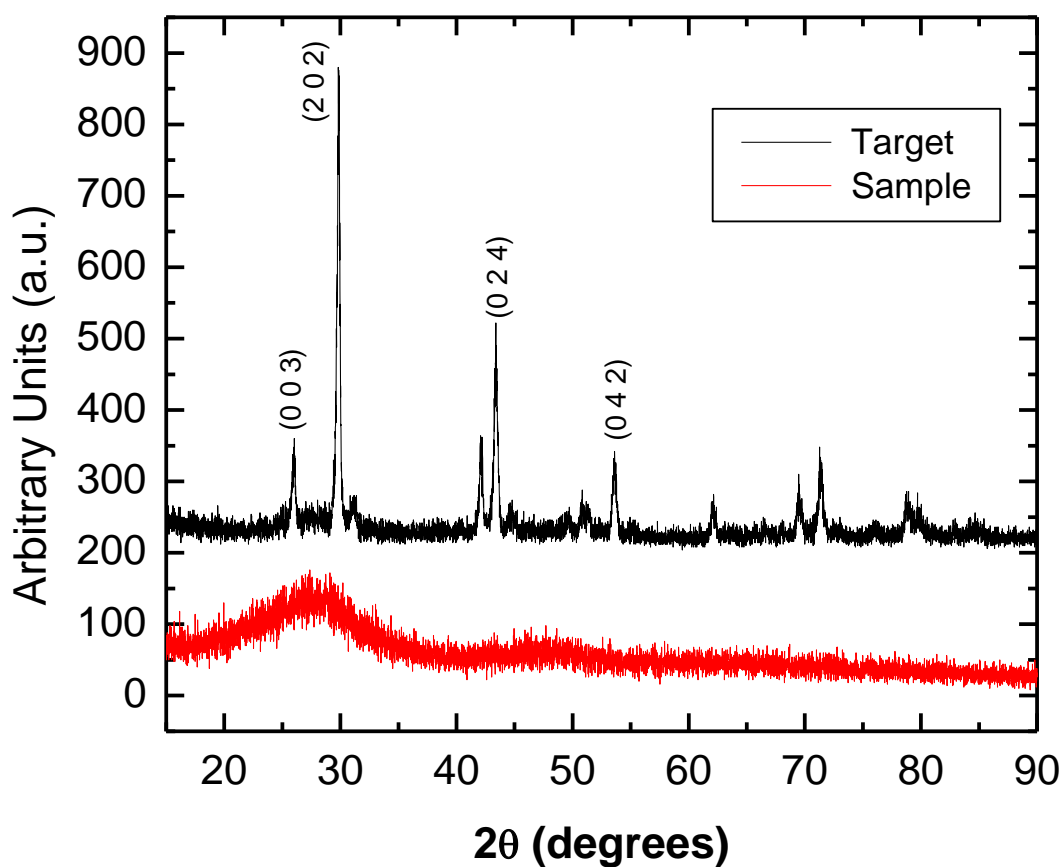


**Figure 4.1. XRD Spectra of GeTe Target and GeTe Thin Film (H1).**

### **A. Effect of Varying the Target to Substrate Distance**

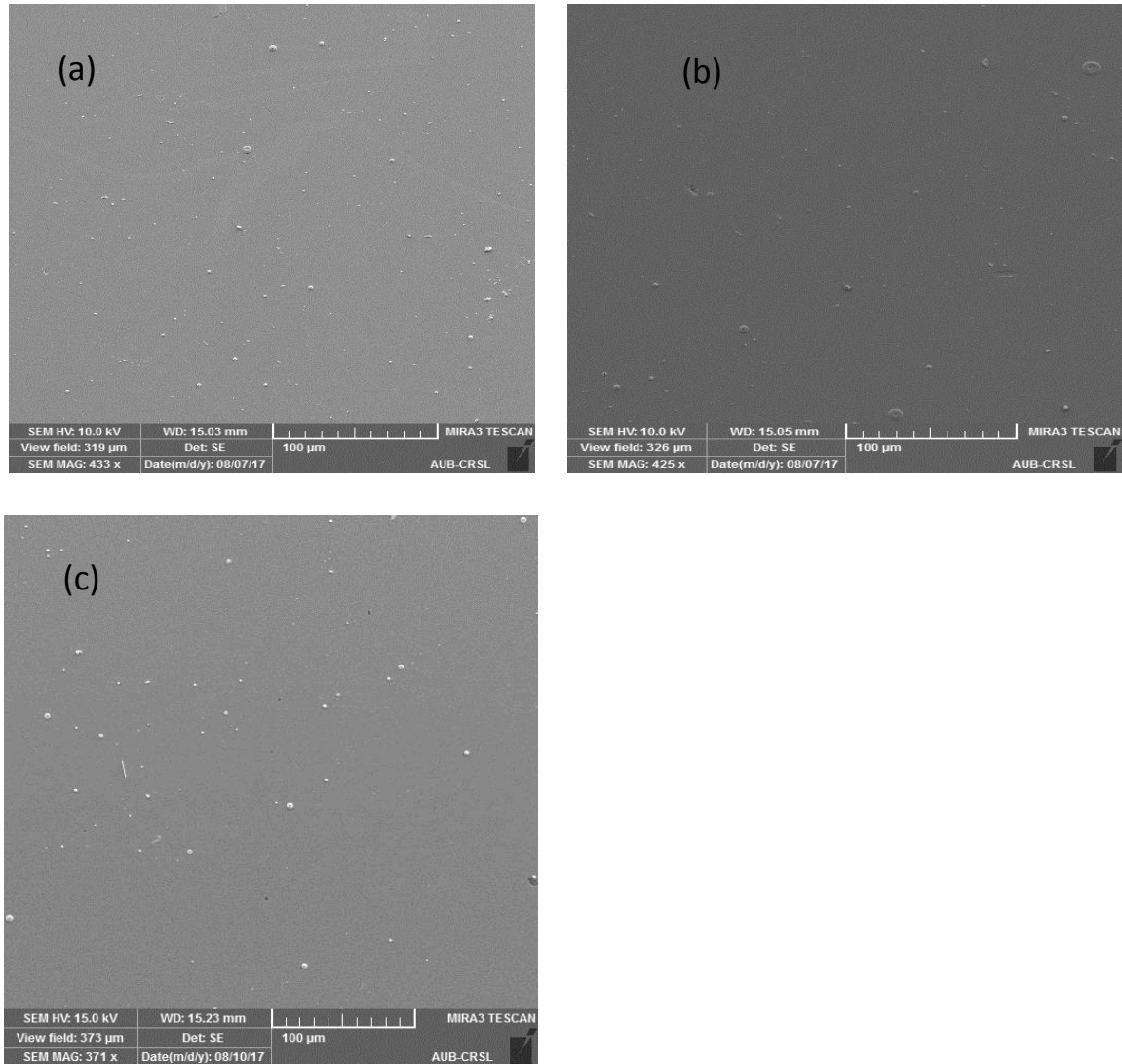
To study the effect of the target to substrate distance on the properties of the deposited GeTe films, four samples were prepared at room temperature.

#### ***1. SEM Images and Discussion***

Fig. 4.2 shows the SEM images for the films H1, H2 and H3, which were deposited at different distances 6, 7 and 10 cm respectively. It is clearly seen that the surfaces of the films appear to be comparably smooth with few droplets. These images



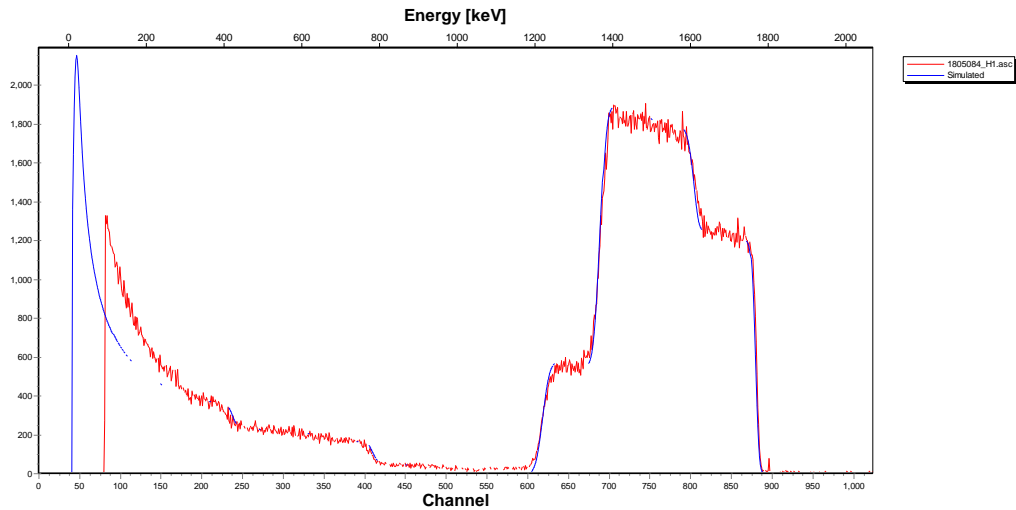
confirmed the absence of delamination and cracks. Droplets are frequently observed during the preparation of films by PLD and could be attributed to splashing of the target depending on the experimental conditions.



**Figure 4.2. SEM Images of the GeTe Films Deposited at Different Target to Substrate Distance. (a) 6, (b) 7, and (c) 10 cm from the target,  $10^{-4}$  mbar of argon pressure, 200 mJ laser energy and 1:30 hours deposition time.**

## 2. Film Composition and Thickness Measurements

Film composition was first estimated using EDX, and most films were found to be quite close to the 50/50 stoichiometry however the error on the measurements in the EDX is up to 10%. In order to get more accurate measurements, the elemental composition, stoichiometry, and thickness of the deposited GeTe thin films were determined using RBS technique, uncertainty on the measurements  $\approx 1\%$ ). The SIMNRA code was used to fit the simulation over experimental data and give information regarding the stoichiometry and film thickness.



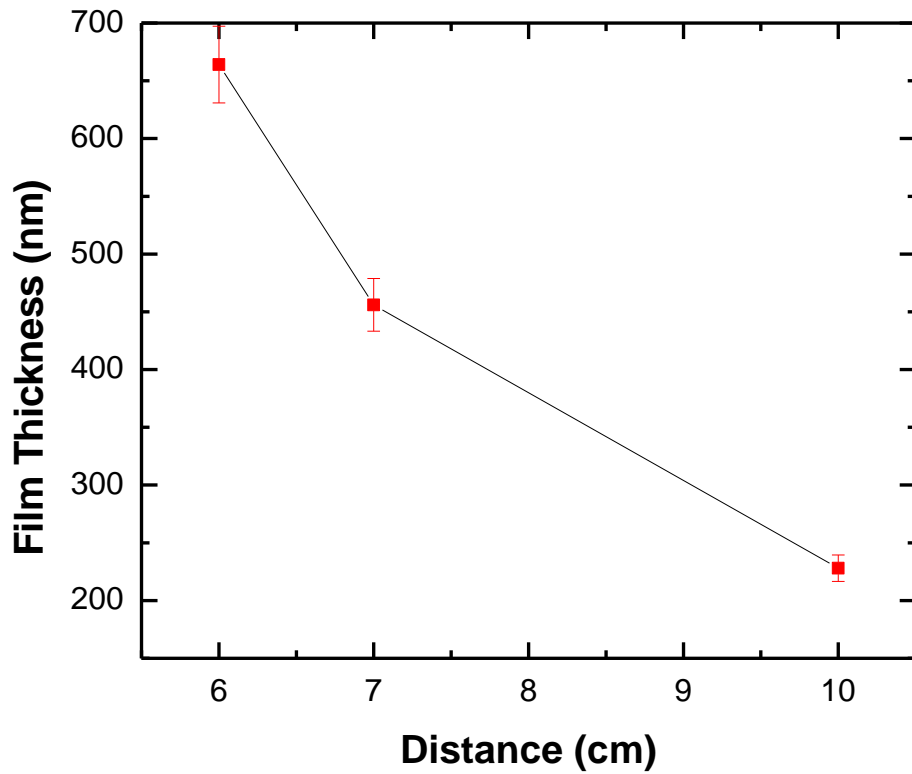
**Figure 4.3. A Typical RBS Spectrum and Simulation for GeTe Thin Film (H1).**

Table 4.1 shows the RBS results, where the atomic composition and thickness of the film at different target-substrate distances are indicated.

**Table 4.1. The Atomic Composition and Thickness of Films Deposited at Different Target to Substrate Distance, where the atomic ratio =  $\frac{\text{atomic \% Ge}}{\text{atomic \% Te}}$**

Sample's name	Distance (cm)	Atomic % Ge	Atomic % Te	Atomic Ratio	Thickness (nm)
H1	6	50.5	49.5	1.02	664
H2	7	50.9	49.1	1.04	456
H3	10	53.7	46.3	1.16	228

The table shows clearly that the thickness of the film decreases with the increase of target to substrate distance as plotted in Fig. 4.4. This is due to the expansion of the laser induced plasma plume with the increase of target–substrate distance. Therefore, the particle flux of the ablated species in the plume over the substrate area decreases with the increase of target–substrate distance which lowers the deposition rate of the GeTe films and hence the thickness [30]. It is also obvious that as we increase the target to substrate distance there is a significant deviation in the composition of the GeTe thin films and thus the atomic ratio. The film obtained at a distance of 6 cm between the target and the substrate is the closest to stoichiometry, whereas the film grown at 10 cm is rich in Ge with a Ge/Te ratio equal to 1.16. This deviation could be due to the difference in atomic masses between Ge and Te.



**Figure 4.4. Variation of the Films' Thickness As a Function of Target to substrate Distance for a Deposition Time of 1:30 Hours and Frequency of 10 Hz.**

### **3. Optical Properties**

The measurement of the absorption coefficient  $\alpha$  as a function of frequency  $\nu$  of the incident beam provides a mean to determine the band gap  $E_g$  of a material. The optical band gap in most of the amorphous semiconductors can be determined using the Tauc relation [31], which is expressed as

$$(\alpha h\nu) = B(h\nu - E_g)^r$$

Where  $B$  is a constant and  $r$  is an index which depends on the nature of electronic transition responsible for the optical absorption. Values of  $r$  for allowed direct and indirect transitions are  $1/2$  and  $2$  respectively [31].

Figure 4.4 shows a Tauc plot of the optical absorption spectrum measured at room temperature for the GeTe film deposited at different target-to-substrate distance. Our results show a linear behavior of  $(\alpha h\nu)^{1/2}$ , which means an indirect transition from the valence to conduction bands. The corresponding indirect energy band gap can be obtained from the intercept of the resulting straight lines with the energy axis, i.e. for  $(\alpha h\nu)^{1/2} = 0$ .

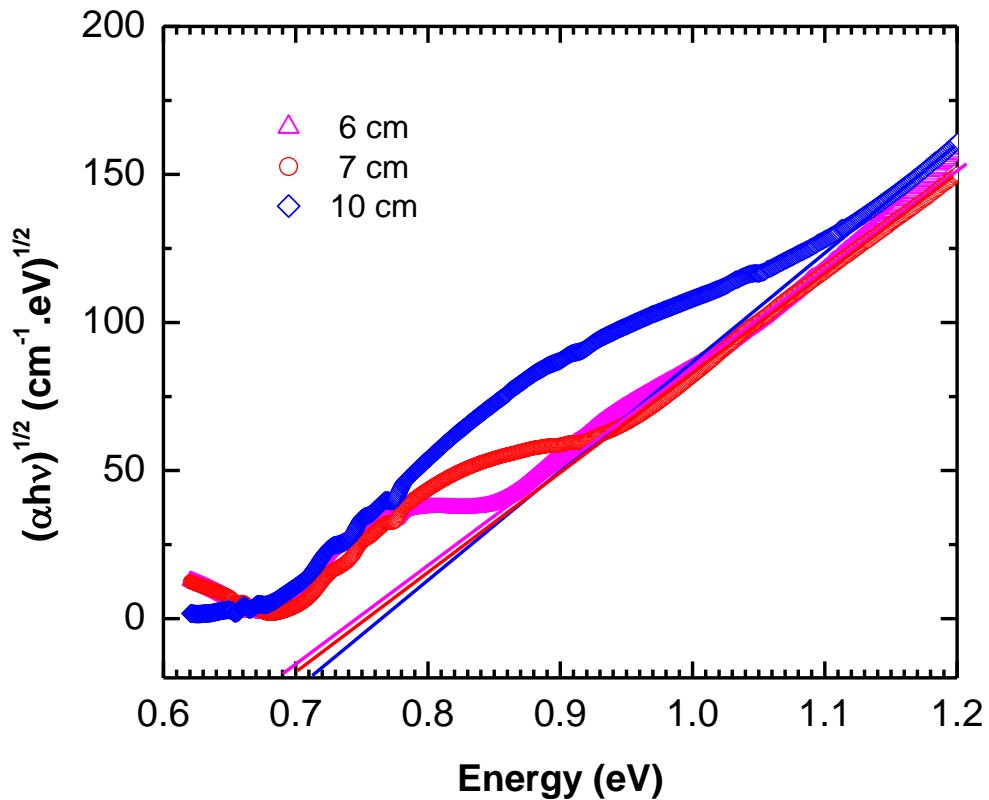


**Figure 4.5. Variation of  $(\alpha h\nu)^{1/2}$  Versus Photon Energy ( $h\nu$ ) for the GeTe Films Deposited under Different Target to Substrate Distance.**

The values of the optical bandgap obtained from Tauc plot are given in table 4.2. Comparing the bandgap values of the three samples deposited at different target to substrate distances, the three samples have a very close value around 0.7 eV

**Table 4.2. The Optical Band Gap of Films Deposited at Different Target to Substrate Distance.**

Sample's name	Distance (cm)	Optical bandgap $E_g$ (eV)
H1	6	$0.69 \pm 0.03$
H2	7	$0.70 \pm 0.04$
H3	10	$0.71 \pm 0.04$

#### ***4. Electrical Properties***

The amorphous-crystalline transition temperatures ( $T_c$ ) and its width have been determined using resistance measurements as a function of temperature for all samples, as plotted on the semi- logarithmic graph in Fig. 4.6. The resistance measurements were carried out on samples H1, H2 and H3 at temperatures between 25 and 270 °C and at a heating rate of 5 K/min.

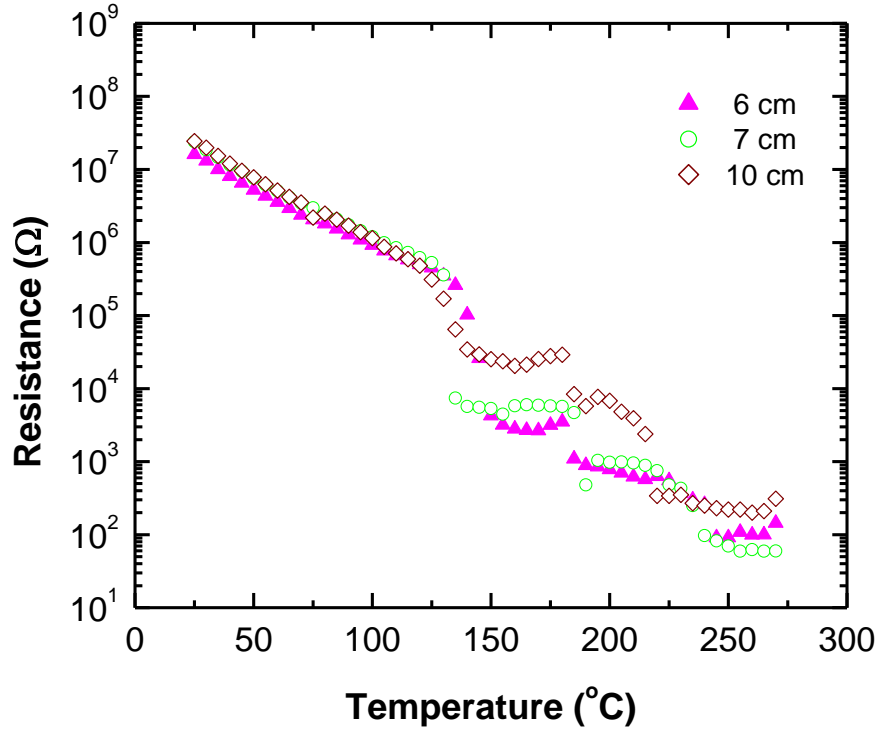


**Figure 4.6. Resistance of the Deposited GeTe Films Measured with Heating Rates of 5 K/min**

As the temperature is raised from 5° to 125 °C, the resistance decreases exponentially; then a sharp drop, encompassing 3 orders of magnitude, is observed over a narrow range. This resistance drop is related to the amorphous to crystalline phase transition, which is mainly due to the increase of mobility, rather than of carrier concentration [26, 32].

According to equation 2.4 and by plotting  $\ln(R)$  as a function of  $1000/T$  (Arrhenius plot), the electrical bandgaps can be determined from the slopes of the curves of figure 4.7. All the electrical results are summarized in table 4.3.

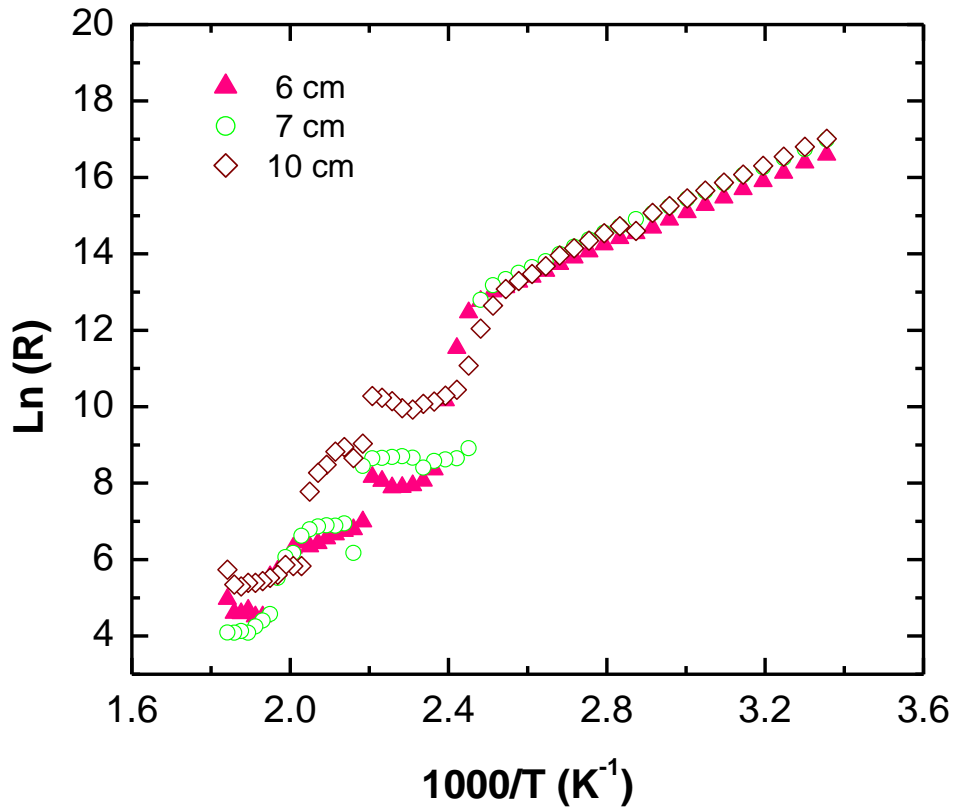


**Figure 4.7. Arrhenius Plots of  $\ln (R)$  Versus  $1000/T$  for GeTe Films Deposited at Different Target to Substrate Distance.**

**Table 4.3. The Crystallization Temperature ( $T_c$ ), Electrical Band Gap ( $E_g$ ), and Transition Width of Films Deposited at Different Target to Substrate Distance.**

Sample's name	Distance (cm)	Electrical $E_g$ (eV)	$T_c$ (°C)	Transition width (°C)
H1	6	$0.74 \pm 0.04$	145	20
H2	7	$0.75 \pm 0.04$	135	10
H3	10	$0.81 \pm 0.04$	140	30



The transition width is defined as the end of the transition subtracted from the beginning of the transition, and the crystallization temperature is:

$$T_c = T_\alpha + \frac{\text{Transition Width}}{2}$$

Where  $T_\alpha$  is the temperature at the beginning of the transition. Several studies were performed to detect the transition temperature of GeTe thin films and the results varied from 150<sup>o</sup> to 255<sup>o</sup> [5, 17, 32, 33, 34 ]. Numerous factors affect this temperature such as deposition technique (PLD, HIND HIVAC coating unit, Atomic Layer Deposition, thermal evaporation), temperature at which films were deposited, film thickness, chamber pressure, deposition time, and heating rate, etc.

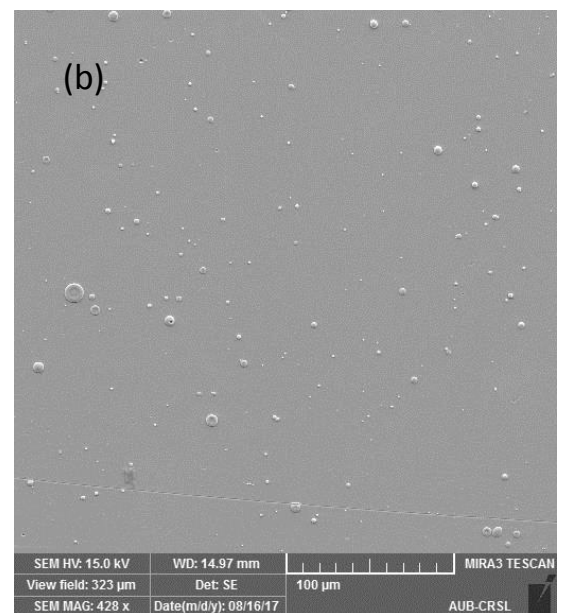
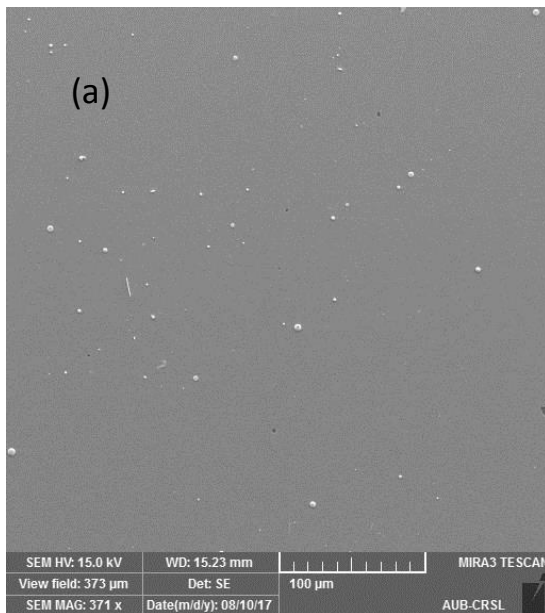
For this set of samples, the band gap has been varied from 0.74 eV to 0.81 eV which is in agreement with the reported band gap of GeTe [35]. However, the variation in the band gap values with upon changing the target to substrate distance is within the experimental error. If we compare the values of the electrical and optical energy gaps, we notice that for all 3 samples the optical band gap is slightly smaller than the electrical one. So, here two different values of threshold for bandgap can be determined, the optical bandgap and electrical bandgap. The optical bandgap is related to the threshold for photons to be absorbed and the electrical bandgap is related to threshold for creating the electron-hole pair [36]. This is mainly relevant in amorphous semiconductors which can have substantial densities of "tail" states, states near the band edge that allow plenty of absorption but little transport, because the states are localized. In such materials the electrical gap is typically larger than the optical one.

## B. Effect of Varying the Deposition Pressure

To study the effect of the Argon pressure on the properties of the deposited GeTe films, four samples were prepared at room temperature.

### 1. SEM Images and Discussion

Fig. 4.8 shows the SEM images for the films deposited in vacuum, and argon pressure of  $10^{-4}$ ,  $10^{-3}$ ,  $10^{-2}$  mbar. Laser



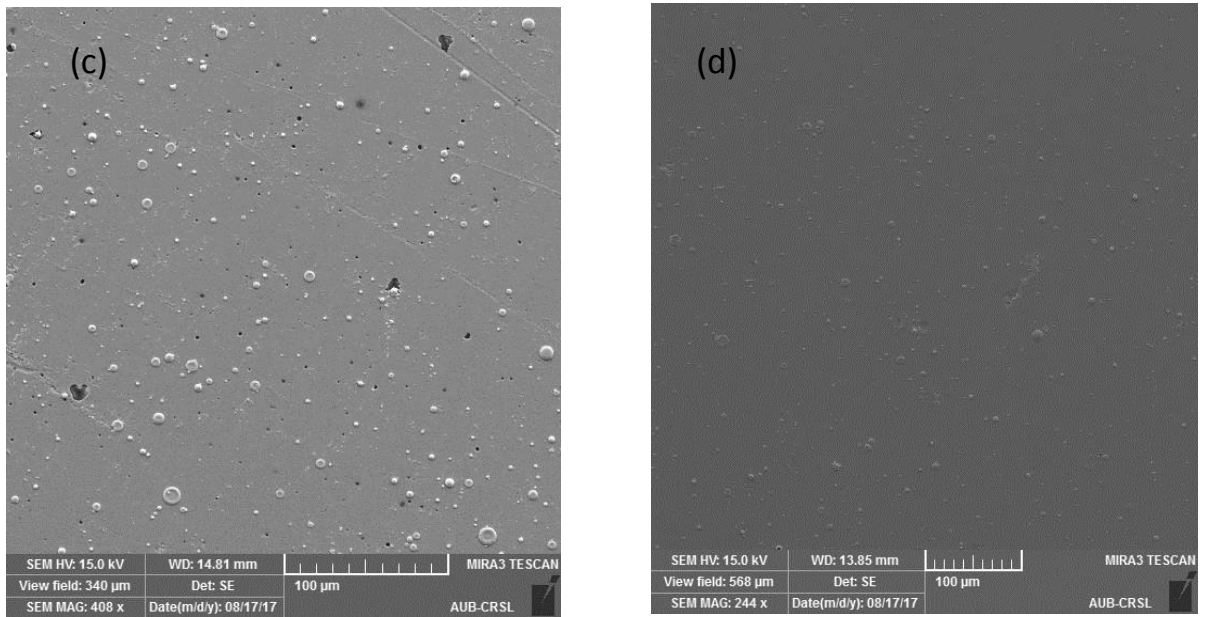


**Figure 4.8. SEM Images of the GeTe Films Deposited in Different Deposition Pressure. (a) vacuum, and pressure of (b)  $1.0 \times 10^{-4}$ , (c)  $1.2 \times 10^{-3}$ , and (d)  $1.0 \times 10^{-2}$ , mbar Argon pressure respectively. Films are deposited at 6 cm target to substrate distance, 200 mJ laser energy and 1:30 hours deposition time.**

From the SEM images, it is clear that the Argon pressure in the chamber influences the surface morphology of the GeTe thin films. The film deposited in vacuum Fig. 4.7 (a) has a smoother surface. The film deposited in Argon atmosphere was rougher compared to the film prepared in vacuum. The change in the surface morphologies were associated to the plasma plume dynamics in a certain atmosphere, the PLD process involves laser beam and target material interaction. Consequently, the plasma plume will be released from the target surface in a perpendicular direction heading toward a substrate. The plasma plume contains ions, electrons, atoms, molecules and clusters. Their kinetic energy is high because of the high energy of the laser beam. In the case of deposition in vacuum, due to absence of a gas, the particles will arrive to the substrate with high kinetic energy and will not encounter collisions with background Argon atoms, atoms will consequently diffuse on the film surface and

smoothen the film. Therefore, the film deposited in the Ar atmosphere were rougher than the films deposited in vacuum and as the background Argon pressure increases the surface of the film becomes rougher. The presence of the chamber gas can greatly change the surface mobility of the arrived particles, and therefore the change in the particles surface mobility may affect the surface morphology [37].

Figures (a), (b) and (c) are homogeneous and crack-free. Yet upon increasing the pressure to the order of  $10^{-2}$  (figure d) cracks clearly appear and thin films lose the homogenous structure thus decreasing the film quality. So, we can conclude that the Argon pressure has a significant impact on the surface morphology of the deposited films; as the background Argon pressure increases the surface of the film becomes rougher.

## ***2. Film Composition and Thickness Measurements***

The influence of the chamber pressure on the film composition and thickness will be studied in the section and the results are summarized in table 4.4.

**Table 4.4. The Atomic Composition and Thickness of Films Deposited at Different Chamber Pressure.**

Sample's name	Ar Pressure (mbar)	Atomic % Ge	Atomic % Te	Atomic Ratio	Thickness (nm)
H4	Vacuum	49.7	50.3	0.99	215
H5	$1.0 \times 10^{-4}$	49.9	50.1	1	614
H6	$1.2 \times 10^{-3}$	51.6	48.4	1.07	600
H7	$1.0 \times 10^{-2}$	48.3	51.7	0.94	304

The thickness of the films was strongly affected by the deposition background gas. The thickness of the films varied for the films deposited in vacuum and different argon pressure. The plume particles dynamics (Kinetic energy, collision, and scattering) plays an important role in determining the film thickness, and they are correlated with the mean free path of the ejected particles [38].

The thinner film recorded for the vacuum environment may be explained by the plume dynamics during the deposition process. In vacuum the plume particles move with their original energy which is very high. These energetic particles, upon reaching the substrate, can induce re-sputtering of the growing layer resulting in thinner layers and smoother surface as shown in Fig. 4.8 (a). In the case of the Ar atmosphere, the lightest particles (ions and atoms) might be slowed down by the Ar atoms, which results in GeTe clusters with enough kinetic energy to stick on the substrate. Consequently, the GeTe films deposited in Argon gas are thicker than the vacuum film. It is also well known that the characteristics of a thin film strongly depend on the pressure of the background gas during PLD, since the ambient particles interact with the particles in the plume [39]. The collision between the ambient gas atoms and the particles in the plume will decrease the kinetic energies of the particles and hence increase the amount of time the particles stay in the plume. This gives the particles enough time to nucleate, agglomerate, and grow into bigger particles prior to their arrival on the substrate [40]. On the other hand, the particles ejected in vacuum moves freely and are expected to have a higher mean free path, and thus, they do not have enough time to nucleate in the plume.

Figure 4.9 indicates the variation of film thickness with the change in Argon pressure. This can be explained as follows: In PLD process under ultrahigh vacuum

conditions deposition, re-sputtering from the film surface occurs due to the presence of energetic particles in the plasma plume, this can be possible by modifying the laser energy density or by modifying the deposition pressure in the chamber. Re-sputtering process involves re-emission of material deposited during the deposition process. Re-emission is caused by ion bombardment of the deposited material. In that case, with increasing argon gas pressure to  $10^{-4}$  mbar, a reduction of the particle energy is accompanied with a decrease of re-sputtering and a rise in the deposition rate. In contrast, for higher gas pressures, scattering of ablated material out of the deposition path between target and substrate is observed, leading to a decrease in the deposition rate.

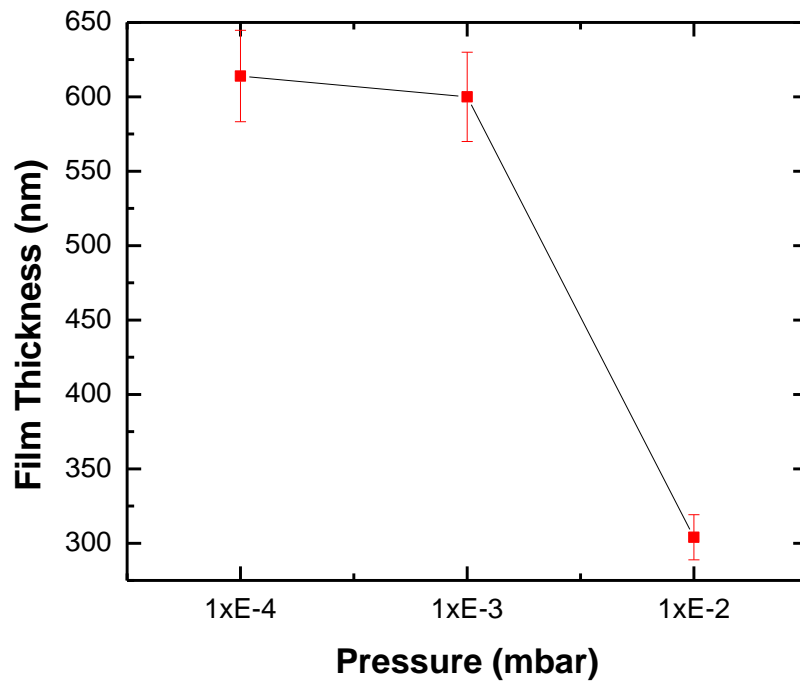


**Fig.4.9. The Variation of Film Thickness As Function of Argon Pressure**

The atomic ratio remains nearly constant ( $\approx 1$ ) for all the samples. Yet of interest, the Ge:Te ratio of the film prepared in vacuum and  $10^{-4}$  mbar pressure is almost 1:1 . This one to one composition starts to fluctuate upon adding Argon gas to the chamber. The deviation of the film composition increases up to 1.66 % upon increasing

the chamber pressure from  $10^{-4}$  to  $10^{-2}$  mbar. This indicates that preparing the films under vacuum or a  $10^{-4}$  mbar Argon pressure will give the best film composition and that the increase in the Ar background pressure will be accompanied with a deviation from the 50:50 composition of the GeTe deposited films.

### 3. Optical Properties

Figure 4.10 shows a Tauc plot of the optical absorption spectrum measured at room temperature for the GeTe film deposited at different Argon pressure.

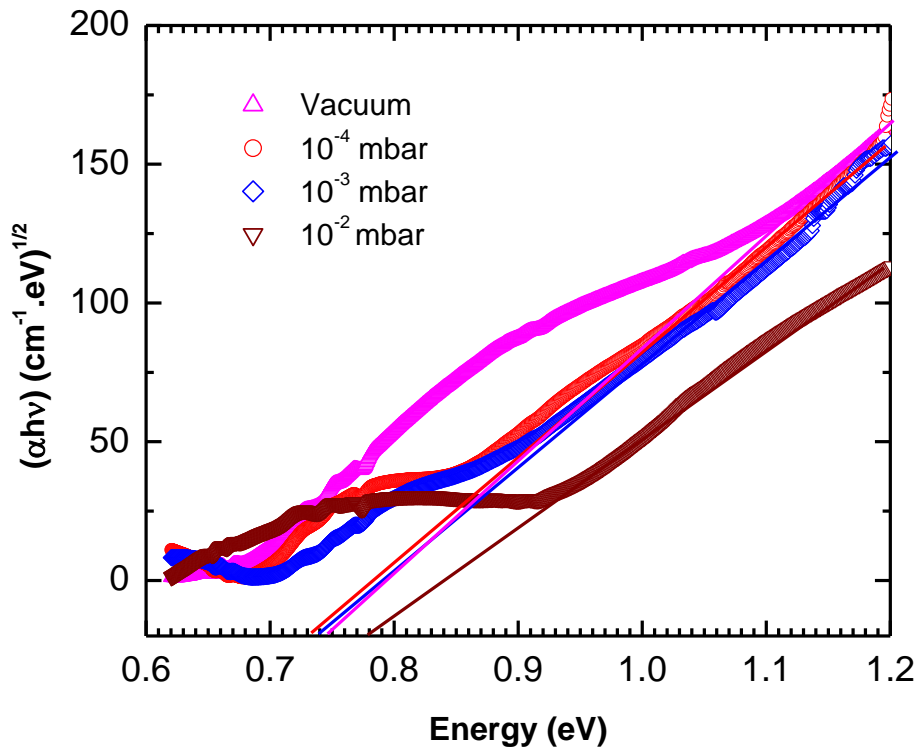


**Figure 4.10. Variation of  $(\alpha hv)^{1/2}$  Versus Photon Energy ( $hv$ ) for the GeTe Films Deposited Under Different Chamber Pressure.**

The same approach, as the one discussed in 4.2.3 has been followed to determine the optical band gap of the 5 samples under study. The results are listed in the table below.

**Table 4.5. The Optical Band Gap of Films Deposited at Different Chamber Pressure.**

Sample's name	Pressure(mbar)	Optical bandgap $E_g$ (eV)
H4	Vacuum	$0.75 \pm 0.04$
H5	$1.0 \times 10^{-4}$	$0.73 \pm 0.04$
H6	$1.2 \times 10^{-3}$	$0.74 \pm 0.04$
H7	$1.0 \times 10^{-2}$	$0.78 \pm 0.04$

The variation of the deposition pressure did not have a significant influence on the optical band gap of the GeTe thin films. The optical band gaps varied between 0.73 and 0.78, however this change lies within the experimental error.

#### 4. Electrical Properties

The resistance measurements were carried out on samples H4, H5, H6 and H7 at temperatures between 25 and 270°C and at a heating rate of 5 K/min.

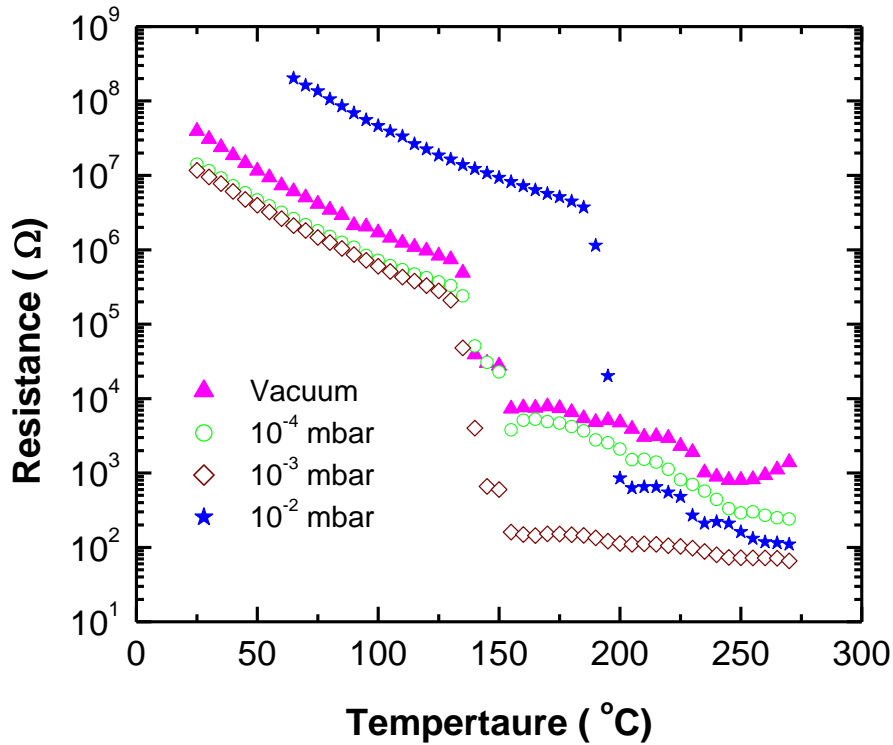


**Fig.4.11. Resistance of the Deposited GeTe films at Different Argon Pressure Measured with Heating Rates of 5 K/min**



In figure 4.12, the electrical band gap of the samples H4, H5, H6, and H7 are determined from the slope of  $\ln(R)$  versus  $1000/T$  and the results are listed in table 4.6. The results are listed in table 4.6.

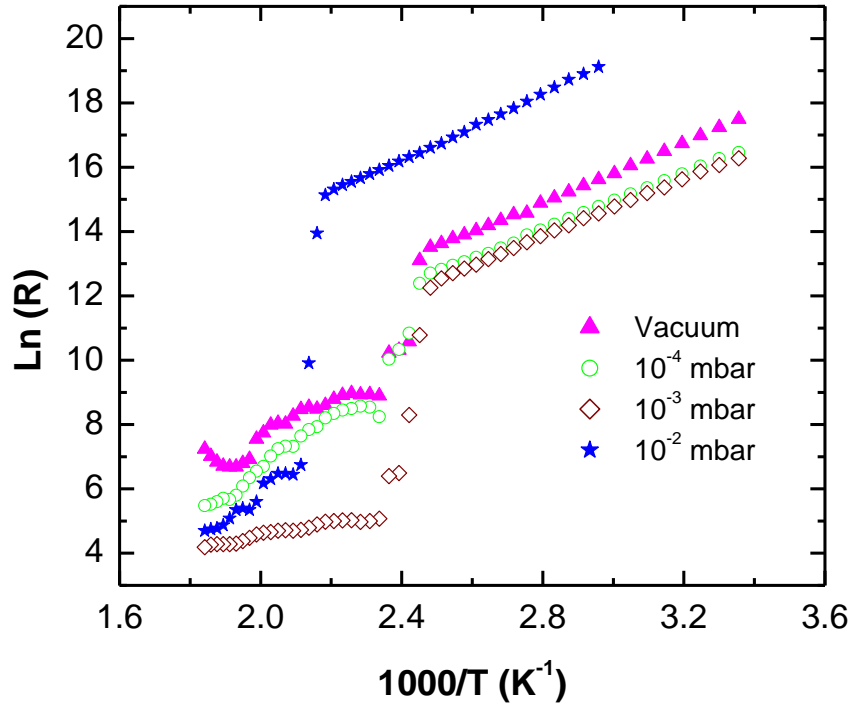


**Fig.4.12. Arrhenius Pots of  $\ln(R)$  Versus  $1000/T$  for GeTe Films Deposited Under Different Argon Pressure.**

**Table 4.6. The Crystallization Temperature ( $T_c$ ), Electrical Band Gap, and Transition Width of Films Deposited at Various Chamber Pressure.**

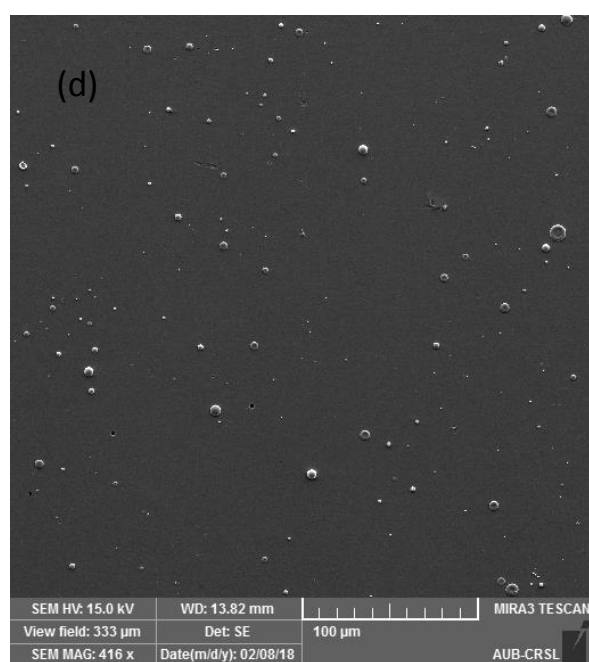
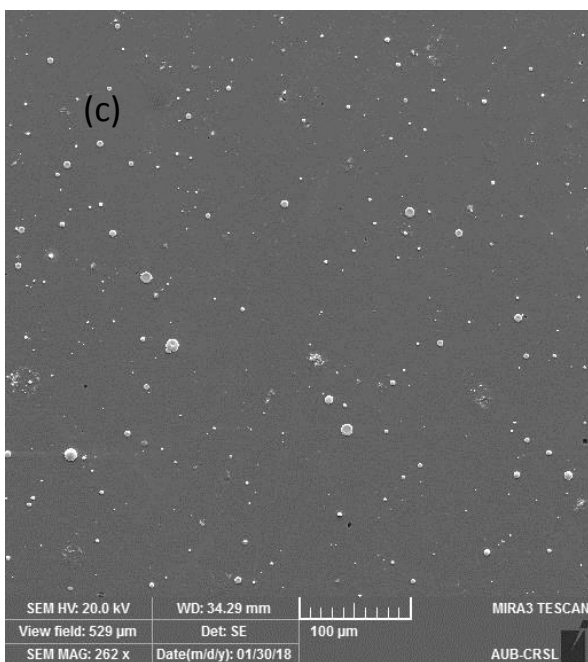
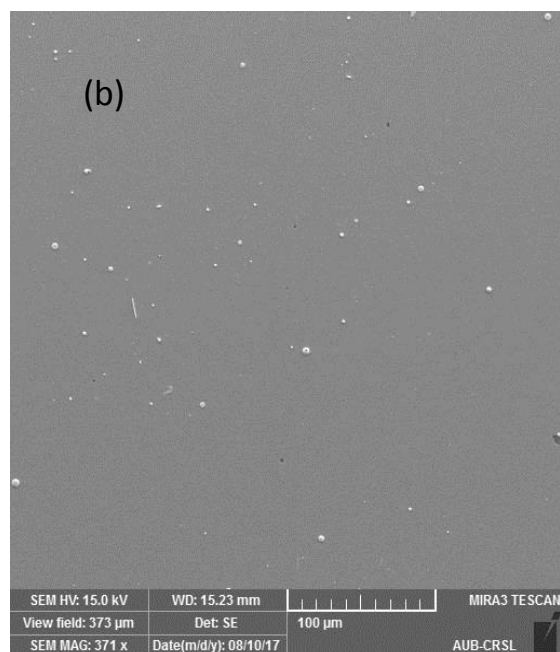
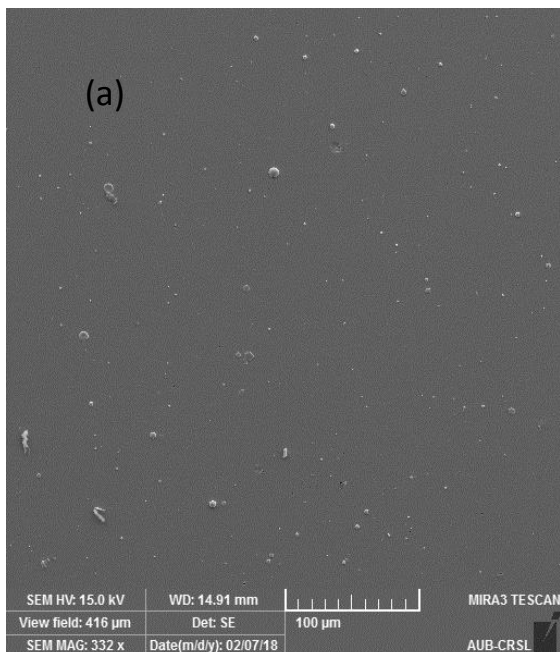
Sample's name	Pressure (mbar)	Electrical $E_g$ (eV)	$T_c$ (°C)	Transition Width (°C)
H4	Vacuum	$0.81 \pm 0.04$	145	20
H5	$1.0 \times 10^{-4}$	$0.74 \pm 0.04$	145	20
H6	$1.2 \times 10^{-3}$	$0.75 \pm 0.04$	143	25
H7	$1.0 \times 10^{-2}$	$0.91 \pm 0.05$	195	20

We notice that the best agreement with the reported band gap (0.742 eV) are samples H5 and H6. The increase of chamber pressure enhances the scattering of Ar particles which reduces the film quality and results in defects in the film. With the increase of collisions between GeTe particles and Argon particles, scattering of ablated material out of the deposition path between target and substrate is observed, leading to a decrease in the deposition rate and thinner films are obtained. All these factors do not favor conduction and thus reduce the quality of the films. It can be also observed that the sample prepared under vacuum does not show agreement with the reported GeTe band gap as well. This can be due to the fact that under vacuum, GeTe particles move freely with very high energy. When these energetic particles reach the substrate, re-sputtering of the previous layer occurs which leads to a thin layer as well.

### **C. Effect Laser Energy**

Laser energy plays an essential role in film formation, for this reason five samples were prepared at different laser energy. These samples were also characterized using the same methodology of the previous parts.

## 1. SEM Images and Discussion



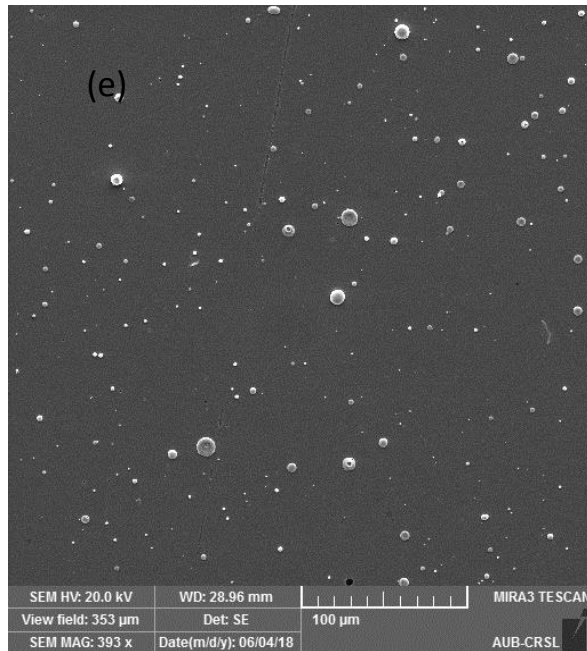


**Fig.4.13. SEM Images of H8, H9, H10, H11 and H12 Samples, the GeTe Films Deposited at Different Laser Energies. (a) 133, (b) 200, (c) 250, (d) 300, and (e) 350 mJ respectively. All images are captured with a scale bar of 100  $\mu\text{m}$ . Films are deposited at 6 cm target to substrate distance,  $10^{-4}$  mbar argon pressure and 1:30 hours deposition time.**

The energy of laser energy on the surface morphology of the GeTe films was studied by scanning electron microscopy. The SEM micrographs of the GeTe films deposited at different energies are shown in figure 4.13. All films are crack free, and droplets do exist (this is a general drawback of the PLD technique). Films prepared at low laser energy are smooth, uniform and compact, while those prepared at higher laser energy contain particulates and clusters in sub-micro size. The formation of the clusters or irregular shape particles can be explained by laser splashing. It is clearly noticed from SEM images that films prepared at energies of 136 and 200 mJ have the best surface morphology and further increasing of the laser energy leads to increasing the density of the clusters and droplets on the grown films.

## 2. Film Composition and Thickness Measurements

Film composition and thickness were investigated using RBS technique and the results are summarized in table 4.7.

**Table 4.7. The Atomic Composition and Thickness of Films Deposited at Different Laser Energies.**

Sample's name	Laser Energy (mJ)	Atomic% Ge	Atomic % Te	Atomic Ratio	Thickness (nm)
H8	136	50.7	49.3	1.03	60
H9	200	50	50	1	241
H10	250	50	50	1	266
H11	300	50.7	49.3	1.03	433
H12	350	51.8	48.2	1.07	560

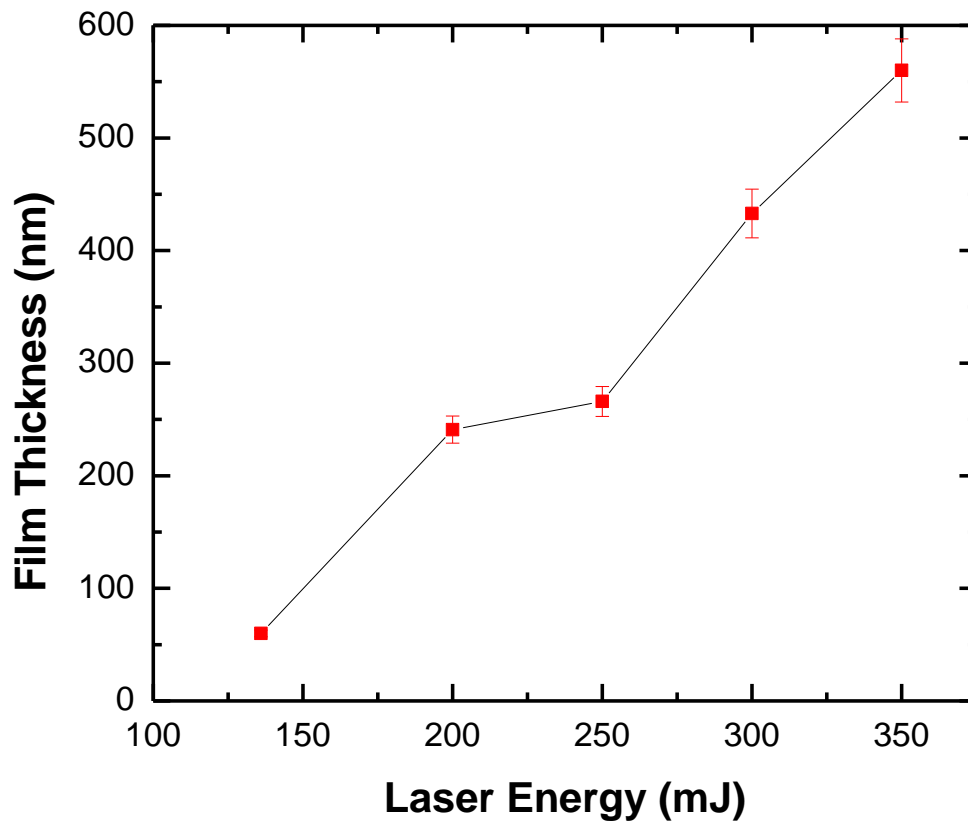


**Figure 4.14. Variation of the Films' Thickness As a Function of Laser Energy**

Figure 4.14 displays the variation of film thickness with laser energy. Thus PLD generally can be divided into four stages.

1. Laser radiation interaction with the target
2. Dynamic of the ablation materials
3. Decomposition of the ablation materials onto the substrate
4. Nucleation and growth of a thin film on the substrate surface

In the first stage, the laser beam is focused onto the surface of the target. At sufficiently high energy density and short pulse duration, all elements in the target surface are rapidly heated up to their evaporation temperature. Materials are dissociated from the target and ablated out with stoichiometry as in the target. The instantaneous ablation rate is highly dependent on the energy of the laser irradiating on the target. Therefore, as we increase the energy of the laser beam, more atoms are removed and thus thickness of the films increases.

It is clear from RBS measurements that the best composition is obtained at laser energy of 200 mJ. The GeTe film composition starts to fluctuate upon increasing the laser energy from 250 to 350 mJ where the deviation from the film composition increases from 0.003% to 1.75%. Similarly, decreasing the energy to 136 mJ will introduce a deviation of 0.7 %. This indicates that preparing the films under a laser energy of 200 mJ will give the best film composition and as we increase or decrease this energy, fluctuations in the Ge:Te ratio start to appear.

### 3. Optical Properties

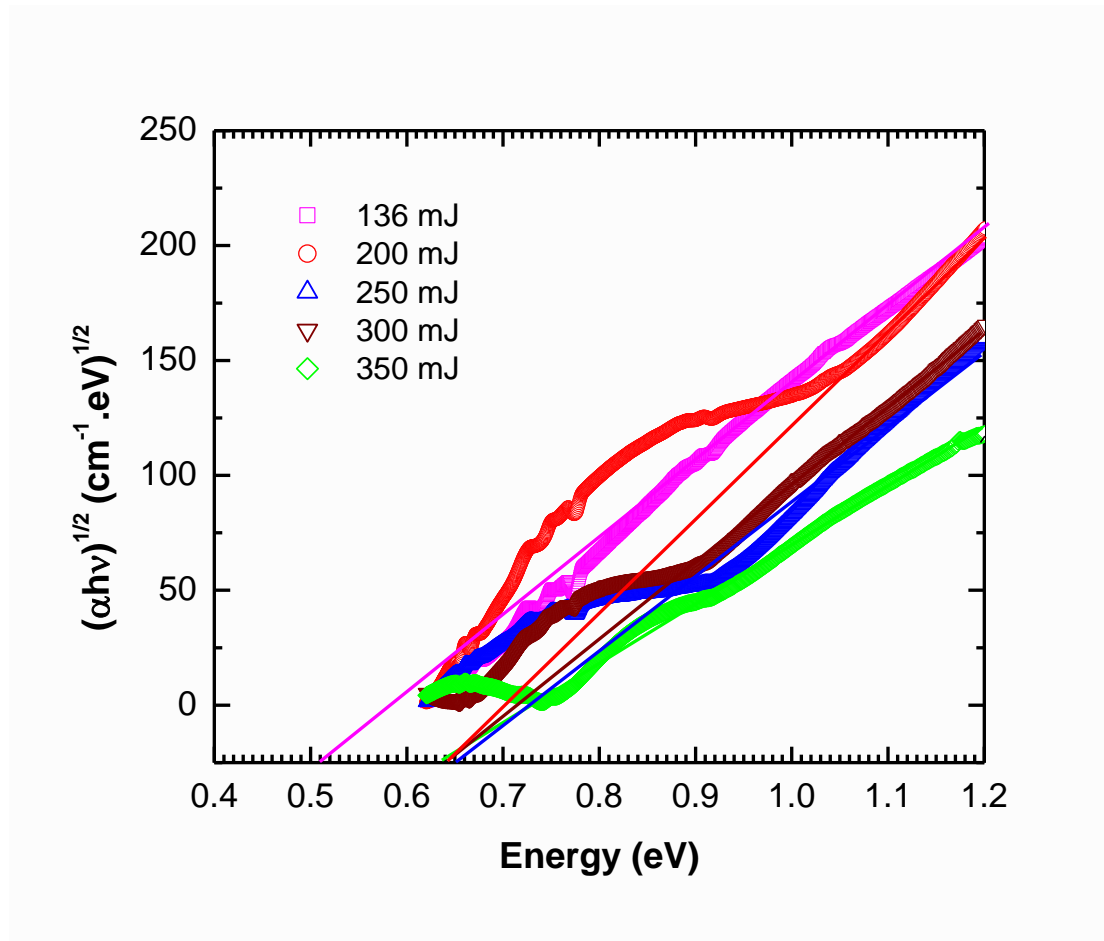


**Figure 4.15. Variation of  $(\alpha h\nu)^{1/2}$  Versus Photon Energy ( $h\nu$ ) for the GeTe Films Deposited Under Various Laser Energies.**

The variation of the optical energy gap with laser energy is given in table 4.8.

**Table 4.8. The Optical Band Gap of Films Deposited at Different Laser Energies.**

Sample's name	Laser energy (mJ)	Optical $E_g$ (eV)
H8	136	$0.51 \pm 0.03$
H9	200	$0.65 \pm 0.03$
H10	250	$0.66 \pm 0.03$
H11	300	$0.64 \pm 0.03$
H12	350	$0.64 \pm 0.03$

#### 4. Electrical Properties

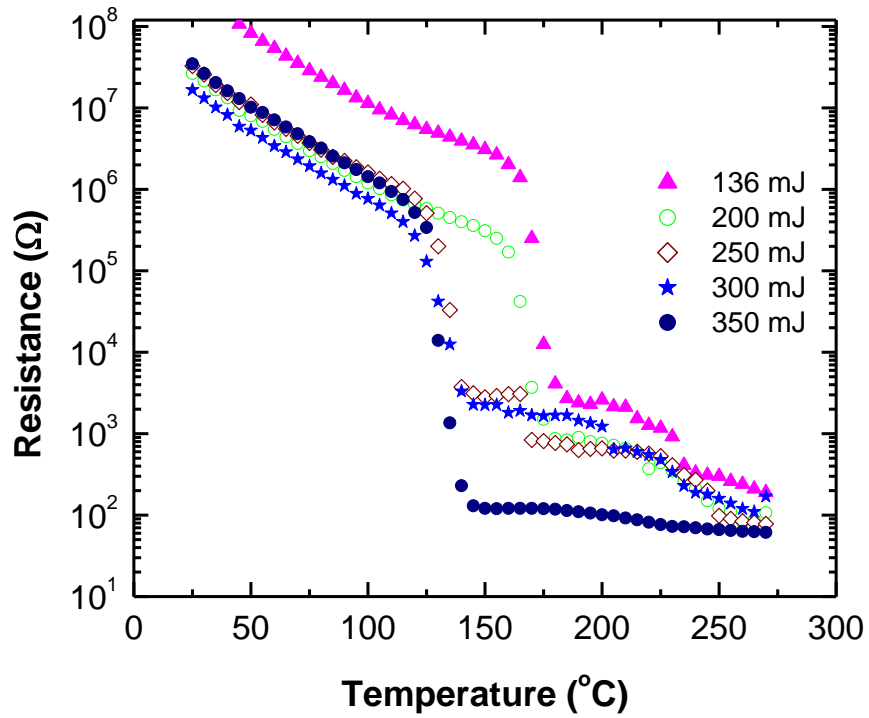


Figure 4.16. Resistance of the Deposited GeTe Films at Different Laser Energies Measured with Heating Rates of 5 K/min

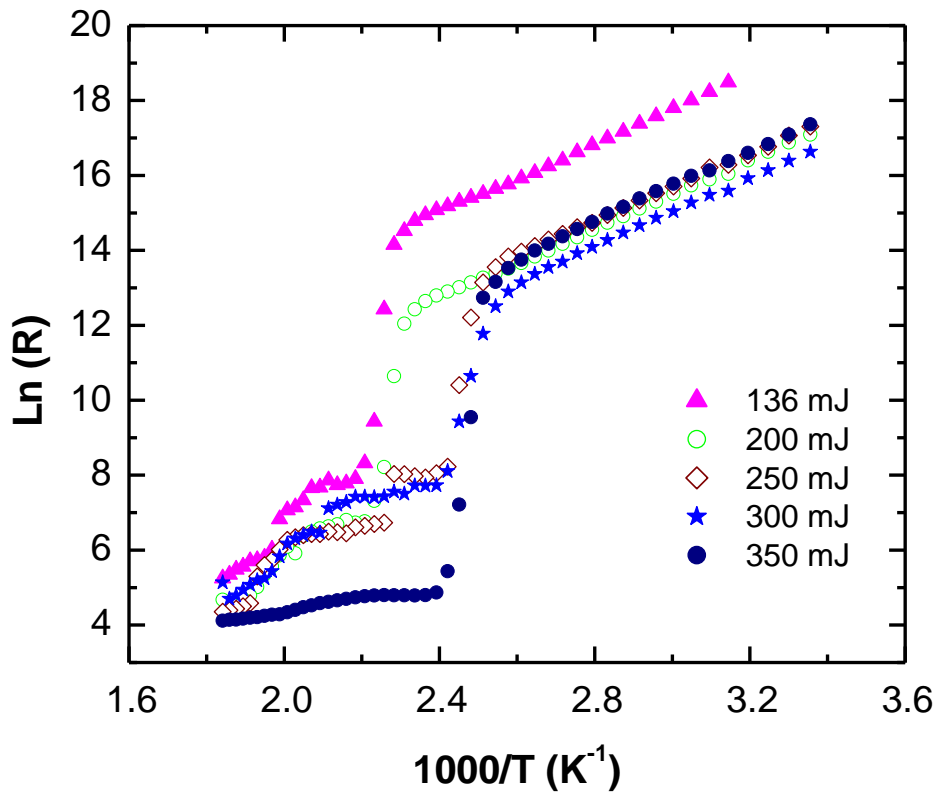


Figure 4.17. Arrhenius plots of  $\ln(R)$  versus  $1000/T$  for GeTe films deposited at different laser energies.



**Table 4.9. The Crystallization Temperature ( $T_c$ ), Electrical Band Gap, and Transition Width of Films Deposited at Various Laser Energies.**

Sample's name	Laser energy (mJ)	Electrical $E_g$ (eV)	$T_c$ (°C)	Transition width (°C)
H8	136	$0.82 \pm 0.04$	175	20
H9	200	$0.78 \pm 0.04$	170	20
H10	250	$0.77 \pm 0.04$	135	20
H11	300	$0.77 \pm 0.04$	133	25
H12	350	$0.77 \pm 0.04$	135	20

The result shows that the phase transition temperature of samples was different upon changing the laser energy. The reported transition temperatures were 175, 170, 135, 133 and 135 °C for samples H8-H12, respectively. It is clear that at low energies (136 and 200 mJ) the transition temperature has higher values compared to those at high energies (250, 300 and 350 mJ). This was previously reported in a study on the influence of laser energy on Ge<sub>2</sub>Sb<sub>2</sub>Te<sub>5</sub> thin films prepared by pulsed laser deposition [41].

The characteristic of PLD is possibly the cause of the above results. PLD is a physical vapor deposition technique that uses the output of a short laser pulse to raise the surface temperature of a small portion of the target and cause a plume of evaporated material to be ejected from the target forming highly disordered amorphous film. However, increasing laser energy will lead to the fact that the plume arriving substrate has redundant energy which will cause part particles to form nuclei or crystals. These nuclei or crystals exist in amorphous film. The crystallization of GeTe includes nucleation and growth. During the process of annealing, the existing nuclei/crystals are helpful to the crystallization of film which explains the decrease in the transition temperature with the increase of laser energy.

The change in laser energy did not have any significant effect on the electrical band gap where all the obtained results are around 0.77 eV.

### 5. Effect of Deposition Time

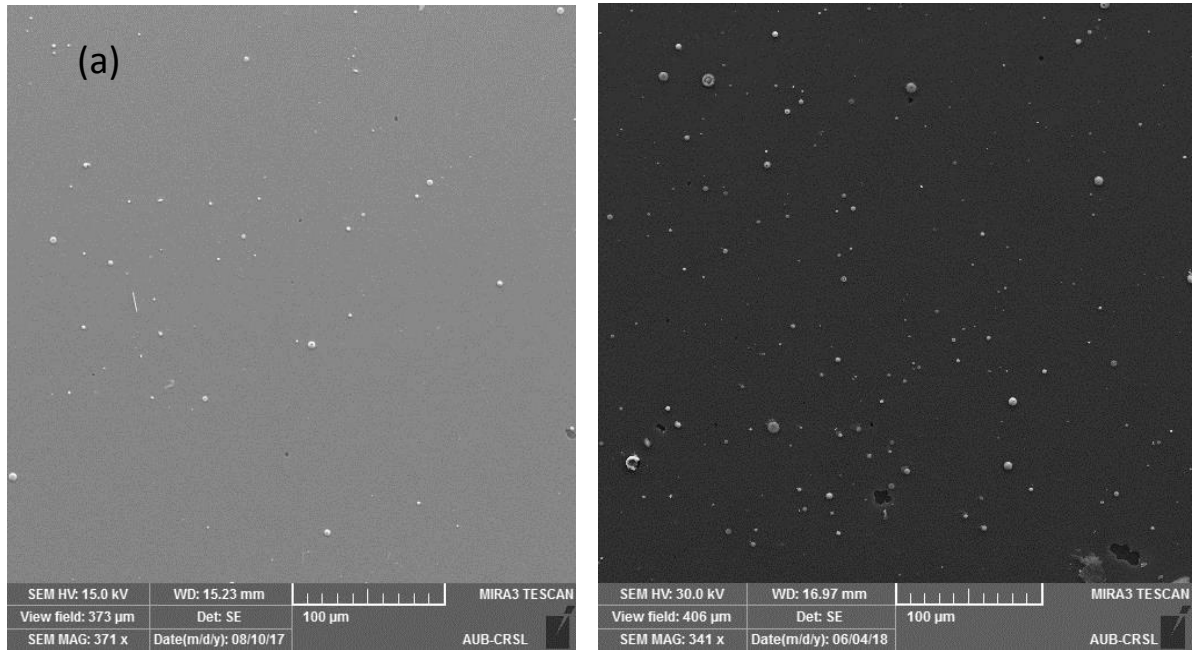


**Figure 4.18. SEM Images of the GeTe Films Are Deposited at Different Time Intervals. (a) 1:30, and (b) 3:30 hours respectively, films are deposited at 6 cm target to substrate distance, 200 mJ laser energy and  $10^{-4}$  mbar argon pressure.**

The aim of this section is to study the influence of changing deposition time on the films prepared, 2 samples are prepared at 1:30 and 3:30 hours.

#### a. SEM Images and Discussion

The thin films prepared for 3:30 hours (fig.4.18 b) are more dense and new particulates are present in comparison with the thin films grown for 1:30 hours (fig.4.18 a) . The growth of thin films starts from a nucleation process: when the nuclei reach a critical size, the grains grow rapidly and an additional growth appears. This additional

growth may affect the direction and the velocity of thin films formation [42]. So we can conclude that the deposition time affects the surface morphology of GeTe thin films; as the deposition time increases the surface of the film becomes rougher.

**b. Film Composition and Thickness Measurements**

Film composition and thickness were investigated using RBS technique and the results are summarized in table 4.10.

**Table 4.10. The Atomic Composition and Thickness of Films Deposited at Different Deposition Intervals.**

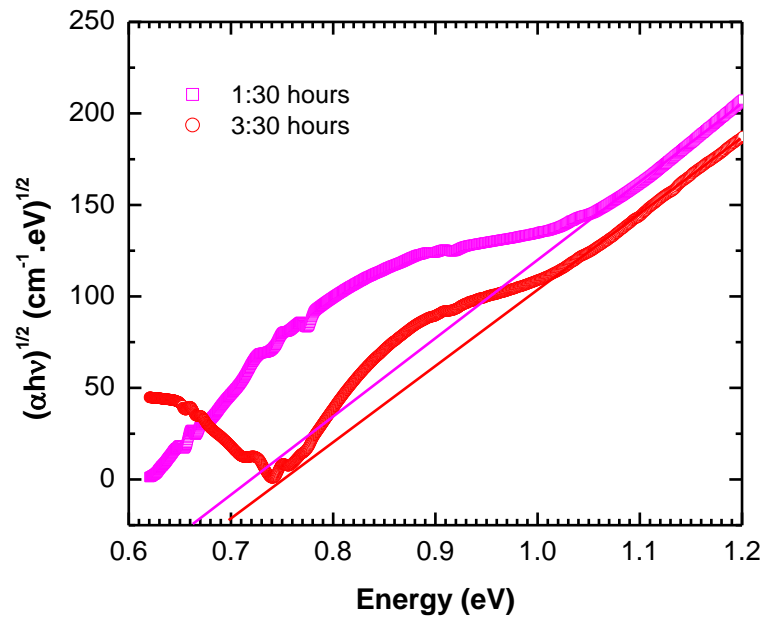
Sample Name	Deposition Time (hrs)	Atomic % Ge	Atomic% Te	Atomic Ratio	Thickness (nm)
H13	1:30	50	50	1	241
H14	3:30	51.6	48.4	1.07	376

Figure 4.19 shows the variation of thickness with deposition time of GeTe films. The film thickness increased from 241 nm to 376 nm as deposition time increases from 90 minutes to 210 minutes. Deposition time has a strong influence on the films' thickness which is an expected result. As deposition intervals increase, more elements in the target surface are heated up to their evaporation temperature and thus more materials are dissociated from the target and ablated out. Therefore, as we increase the deposition time, more atoms are removed and thus thickness of the films increases.

It is noticed from table 4.10 that the best film composition is obtained at a 90 minutes deposition interval where the Ge: Te ratio obtained is 1 to 1. The increase in deposition time introduces a deviation from stoichiometry (1.61%); as the thickness of the film increased, the atomic percentage of Ge increases while those of Te

decreased. The deviation from stoichiometry upon increasing film thickness was previously recorded in thin films [42, 43, 44]. From this it may be confirmed that the atomic percentage of the thin films is altered as the films are prepared at different duration time and thus we can conclude that a deposition time of 90 minutes will give the best film stoichiometry.

c. Optical Properties



**Figure 4.19. Variation of  $(\alpha h\nu)^{1/2}$  Versus Photon Energy ( $h\nu$ ) for the GeTe Films Deposited Under Various Deposition Intervals.**

**Table 4.11. The Optical Band Gap of films Deposited at Different Deposition Time.**

Sample Name	Deposition Time (hrs)	Optical $E_g$ (eV)
H13	1:30	$0.66 \pm 0.03$
H14	3:30	$0.70 \pm 0.04$

The values of the optical bandgap accompanied with the increase in the deposition time are previously reported [45] and fall within the experimental error.

d. Electrical Properties

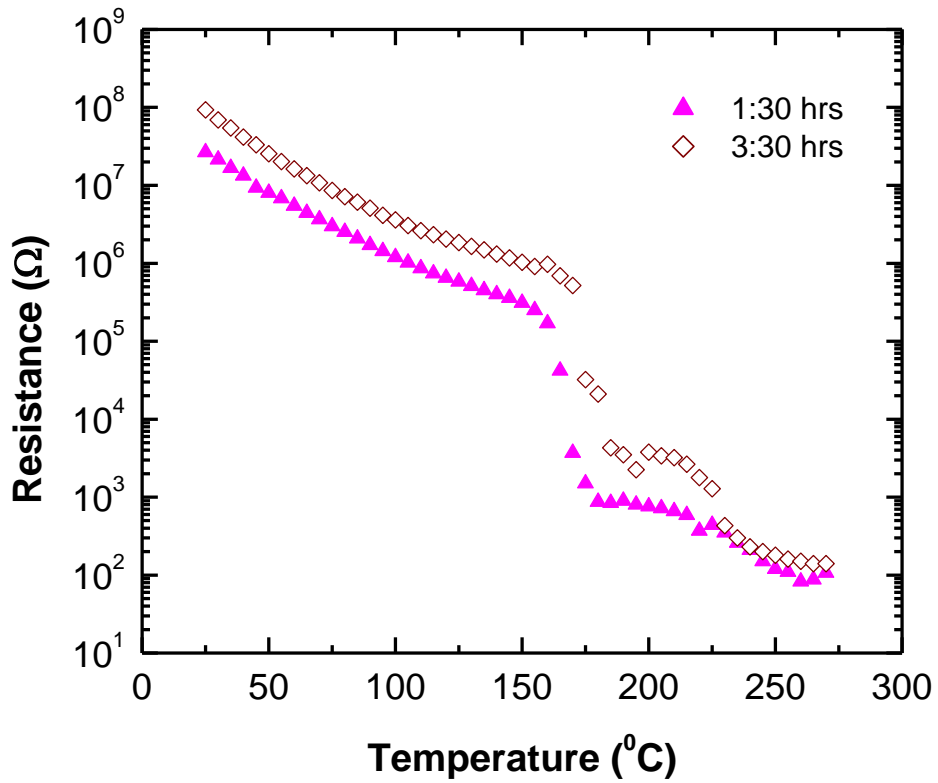


**Figure 4.20. Resistance of the Deposited GeTe films at Different Deposition Intervals Measured with Heating Rates of 5 K/min**

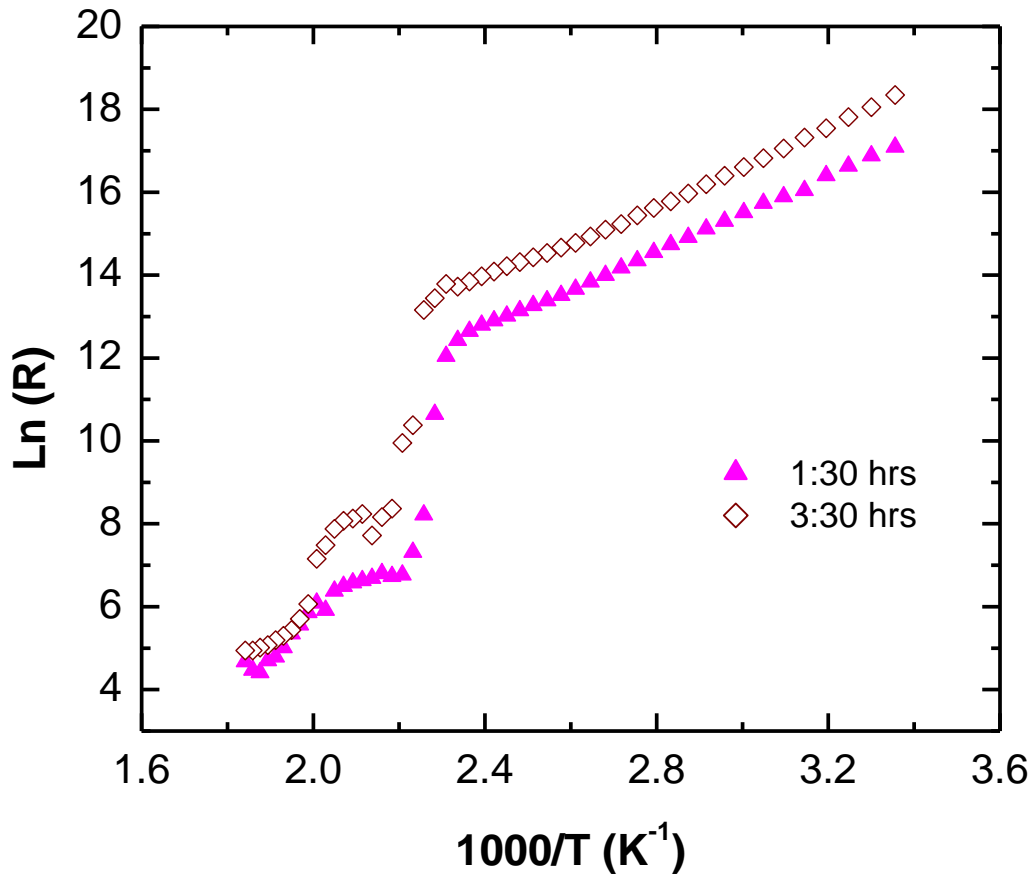


**Figure 4.21. Arrhenius Plots of  $\ln(R)$  Versus  $1000/T$  for GeTe Films Deposited at Different Deposition Intervals.**

The results of the electrical measurements are summarized in table 4.12.

**Table 4.12. The Crystallization Temperature ( $T_c$ ), Electrical Band Gap, and Transition Width of Films Deposited at Various Deposition Times.**

Sample Name	Deposition Time (hrs)	Electrical $E_g$ (eV)	$T_c$ ( $^{\circ}C$ )	Transition Width ( $^{\circ}C$ )
H13	1:30	$0.78 \pm 0.04$	170	20
H14	3:30	$0.84 \pm 0.03$	180	20

The obtained electrical band gaps are 0.78 eV and 0.84 eV at deposition time of 1:30 and 3:30 hours respectively. However, these values lie within the experimental error. The values of both the transition temperature and transition width are reasonable.

From the resistance-temperature curves, we observe two or more transitions. The sharpest one (first transition) represents the amorphous-crystalline transition as mentioned above. The other could be certain transitions from metastable phase to a stable one in the crystal structure. Four possible crystal structures: R3m, P1, Cm, and Fm3m can coexist in crystalline GeTe where Cm transforms into P1 or R3m after laser irradiation [45]. In order to explore those phases, XRD measurements as a function of temperature are needed. Unfortunately, this technique is not available in our lab.

## CHAPTER 5

### CONCLUSION

In this work, we accomplished the growth of GeTe thin films by laser ablation and investigated their physico-chemical properties as a function of experimental parameters namely target to substrate distance, deposition pressure and laser energy.

The experimental techniques employed were X-Ray Diffraction (XRD) for studying the crystalline quality, Scanning Electron Microscopy (SEM) for imaging the surface of the films, Rutherford Backscattering technique (RBS) to determine their chemical composition and thickness. In addition, UV-VIS- NIR spectroscopy was used to measure the optical band gap of the deposited films. Finally, the measurement of the sheet resistance as a function of temperature using two probe method allowed us to determine the amorphous to crystalline transition temperature of the thin films as well as their electrical energy gap.

Our results have led to the following conclusions:

Increasing the target to substrate distance from 6 to 10 cm lead to a decrease in deposition rate and a noticeable deviation of 3.75% in the film stoichiometry. The change in the optical and electrical band gaps were within the experimental errors where the values of the optical energy gap is slightly smaller than the electrical one.

Deposition under Argon pressure greatly influences the surface morphology of the films; upon increasing the pressure to  $10^{-2}$  mbar (maximum pressure used in this work), cracks clearly appear and thin films lose the homogenous structure. Film stoichiometry is little affected by pressure, but the film thickness decreased at higher



pressure respectively. The film deposited at  $10^{-2}$  mbar shows a relatively high transition (195°C) temperature compared to films deposited at lower pressure ( $\approx 140$  °C).

Films prepared at low laser energy are smooth, and uniform, while those prepared at higher laser energy contain particulates and clusters in sub-micro size. The increase in laser energy leads to higher deposition rate but little deviation in the film stoichiometry and band gap.

Furthermore, increasing deposition time leads to an increase in film thickness but rougher films. The change in electrical and optical band gaps is within the experimental error.

The GeTe films deposited at 6 cm target to substrate distance, 200 mJ laser energy,  $10^{-4}$  mbar argon pressure and 1:30 hours of deposition gives the best film conditions due to the smooth surface morphology, 50 to 50 composition, acceptable band gaps, transition temperature and width.

As for future work, there are two main issues that require further investigation. The effect of adding certain metals to the GeTe target and its impact on the deposited thin films would be an interesting follow-up to this work. It is also of great importance to go into the details and investigate the multi-transitions obtained in the resistance versus temperature curves and compare the results with those obtained from Raman spectra measurements.

## APPENDICES

## APPENDIX A

### LIST OF FILMS DEPOSITED IN THIS WORK

Sample Name	Distance	Ar Pressure (mbar)	Laser Energy (mJ)	Deposition Time (hrs)	Frequency (Hz)
H1	6	$1.4 \times 10^{-4}$	200	1:30	10
H2	7	$1.4 \times 10^{-4}$	200	1:30	10
H3	10	$1.9 \times 10^{-4}$	200	1:30	10
H4	6	Vacuum	200	1:30	10
H5	6	$1.0 \times 10^{-4}$	200	1:30	10
H6	6	$1.2 \times 10^{-3}$	200	1:30	10
H7	6	$1.0 \times 10^{-2}$	200	1:30	10
H8	6	$1.9 \times 10^{-4}$	136	1:30	10
H9	6	$2.2 \times 10^{-4}$	200	1:30	10
H10	6	$1.6 \times 10^{-4}$	250	1:30	10
H11	6	$1.4 \times 10^{-4}$	300	1:30	10
H12	6	$1.6 \times 10^{-4}$	350	1:30	10
H13	6	$2.2 \times 10^{-4}$	200	1:30	10
H14	6	$1.4 \times 10^{-4}$	200	3:30	10

## REFERENCES

- Adkins, L. (2004). *Empires of the plain: Henry rawlinson and the lost languages of babylon*. London: Harper perennial.
- Zalden, P. E. (2012). *Phase-Change Materials: Structure, vibrational states and thermodynamics of crystallization*.
- Wuttig, M., & Yamada, N. (2007). Phase-change materials for rewriteable data storage. *Nature Materials*, 6(11), 824-32
- M. Anbarasu & Wuttig, M. (2011). Understanding the Structure and Properties of Phase Change Materials for Data Storage Applications. *Journal of the Indian Institute of Science VOL 91:2*
- Sangeetha, B. G., Rahman, M. R., Akash, A., Govind, S., Santosh, K. S., Sumana, S., Suresh, K. (2015). Preparation and switching studies on binary compound GeTe for memory applications. *Materials Today: Proceedings*, 2(4-5), 1435-1440.
- Ovshinsky, S. R. (1968). Reversible electrical switching phenomena in disordered structures. *Physical Review Letters*, 21(20), 1450-1453.
- Wong, H. P., Raoux, S., Kim, S., Liang, J., Reifenberg, J. P., Rajendran, B., Goodson, K. E. (2010). Phase change memory. *Proceedings of the IEEE*, 98(12), 2201-2227.
- Raoux, S. (2009). Phase change materials. *Annual Review of Materials Research*, 39(1), 25-48.
- Luckas, J., Piarristeguy, A., Bruns, G., Jost, P., Grothe, S., Schmidt, R. M., Wuttig, M. (2013). Stoichiometry dependence of resistance drift phenomena in amorphous GeSnTe phase-change alloys. *Journal of Applied Physics*, 113(2), 23704-7.
- Maeda Y., Andoh, H., Ikuta, I., & Minemura, H. (1988). Reversible phase-change optical data storage in InSbTe alloy films. *Journal of Applied Physics*, 64(4), 1715.
- Sarnet, T., Pore, V., Hatanpää, T., Ritala, M., Leskelä, M., Schrott, A., Cheng, H. (2011). Atomic layer deposition and characterization of GeTe thin films. *Journal of the Electrochemical Society*, 158(12), D694
- Howard, W. E., & Tsu, R. (1970). Photoconductivity and density of states for amorphous GeTe. *Physical Review B*, 1(12), 4709-4719
- Edwards, A. H., Pineda, A. C., & Umrigar, C. J. (2006). Electronic structure of intrinsic defects in crystalline germanium telluride. *Physical Review B*, 73(4)

- Luckas, J.M. (2012). Transport électronique dans les matériaux amorphes à changement de phase (Doctoral dissertation). ÉCOLE DOCTORALE : Sciences et Technologies de l'Information des Télécommunications et des Systèmes.
- Khoo, C. Y., Liu, H., Sasangka, W. A., Made, R. I., Tamura, N., Kunz, M., Thompson, C. V. (2016;2015;). Impact of deposition conditions on the crystallization kinetics of amorphous GeTe films. *Journal of Materials Science*, 51(4), 1864-1872.
- Eason, R. (2007). Pulsed laser deposition of thin films: Applications-led growth of functional materials. Hoboken, N.J: Wiley-Interscience
- Sun, X. (2017). Phase Transformations and Switching of Chalcogenides Phase Change Material Films Prepared by Pulsed Laser Deposition (Doctoral dissertation). Universität Leipzig
- Zalden, P. E. (2012). Phase-Change Materials: Structure, vibrational states and thermodynamics of crystallization.
- Meinders, E. R., & SpringerLink (2006). Optical data storage: Phase-change media and recording. Dordrecht: Springer.
- Yamada, N., Ohno, E., Akahira, N., Nishiuchi, K. I., Nagata, K. I., & Takao, M. (1987). High speed overwriteable phase change optical disk material. *Japanese Journal of Applied Physics*, 26(S4), 61.
- Wang, L., Tu, L., & Wen, J. (2017). Application of phase-change materials in memory taxonomy. *Science and Technology of advanced MaTerialS*, 18(1), 406-429.
- Omar, M. A. (1975). Elementary solid state physics: principles and applications. Pearson Education India.
- Sebastian, I., Divya, S., Nampoore, V. P. N., Radhakrishnan, P., & Thomas, S. (2013). Impact of intermediate localized states on nonlinear optical absorption of ga-ge-ge nanocolloidal solutions. *Applied Physics Letters*, 102(3)
- Kastner, M., Adler, D., & Fritzsche, H. (1976). Valence-alternation model for localized gap states in lone-pair semiconductors. *Physical Review Letters*, 37(22), 1504-1507
- P. G. Le Comber. (1979). Electrical conduction in amorphous semiconductors. *Science Progress (1933- )*, 66(261), 105-118.
- Krebs, D. (2010). Electrical transport and switching in phase change materials.
- Chrissey, D. B., & Hubler, G. K. (1994). *Pulsed laser deposition of thin films*. New York: Wiley.

- Abi Akl, M. N. (2009). Phase Control of Manganese Dioxide Thin Films by Plasma Assisted Laser Ablation. Master's Thesis. American University of Beirut, Lebanon.
- Prasad, P. N. (2004). *Growth and Characterization of Nanomaterials*, in *Nanophotonics*. USA, New Jersey, Hoboken: John Wiley & Sons, Inc.
- Mostako, A. T. T., & Khare, A. (2012). Effect of target–substrate distance onto the nanostructured rhodium thin films via PLD technique. *Applied Nanoscience*, 2(3), 189-193.
- Tauc, J. (1968). Optical properties and electronic structure of amorphous Ge and Si. *Materials Research Bulletin*, 3(1), 37-46.
- Sangeetha, B. G., Rahman, M. R., Akash, A., Govind, S., Santosh, K. S., Sumana, S Suresh, K. (2015). Preparation and switching studies on binary compound GeTe for memory applications. *Materials Today: Proceedings*, 2(4-5), 1435-1440
- Song, K., Beak, S., & Lee, H. (2010). Amorphous-to-crystalline phase transition of [ thin films. *Journal of Applied Physics*, 108(2), 024506.
- Kumar, P., Thangaraj, R., & Sathiaraj, T. S. (2011). Electrical and optical study of phase transitions in thermally evaporated GeTe films. *Physica Status Solidi (a)*, 208(4), 838-842.
- Palaz, S., Koc, H., Mamedov, A. M., & Ozbay, E. (2017). Topological insulators: Electronic band structure and spectroscopy. *IOP Conference Series: Materials Science and Engineering*, 175, 12004.
- Fritzsche, H. (1971). Optical and electrical energy gaps in amorphous semiconductors. *Journal of Non-Crystalline Solids*, 6(1), 49-71. doi:10.1016/0022-3093(71)90015-9
- Norton, D. P., Park, C., Budai, J. D., Pennycook, S. J., & Prouteau, C. (1999). Plume-induced stress in pulsed-laser deposited CeO<sub>2</sub> films. *Applied Physics Letters*, 74(15), 2134-2136.
- Hasabeldaim, E., Ntwaeaborwa, O. M., Kroon, R. E., Motaung, D. E., Coetsee, E., & Swart, H. C. (2017). Effect of PLD growth atmosphere on the physical properties of ZnO: Zn thin films. *Optical Materials*, 74, 76-85.
- Savchuk, V., Kotlyarchuk, B., & Oszwaldowski, M. (2005). Production of indium doped zinc oxide thin films by pulsed laser ablation
- Liu, M., Man, B. Y., Xue, C. S., Zhuang, H. Z., Zhu, H. C., Wei, X. Q., & Chen, C. S. (2006). The effect of nitrogen pressure on the two-step method deposition of GaN films. *Applied Physics A*, 85(1), 83-86

- Hu, D. Z., Pan, F. M., Lu, X. M., & Zhu, J. S. (2011). Influence of laser energy on the crystallization of Ge<sub>2</sub>Sb<sub>2</sub>Te<sub>5</sub> thin film prepared by pulsed laser deposition. *Physica Status Solidi (a)*, 208(12), 2749-2752.
- Jeong, J. (2015). Effect of the change of deposition time on the secondary direction and abnormal shape of grains growth of SnO<sub>2</sub> thin films. *Advances in Materials Science and Engineering*, 2015.
- Baig, M. K., Atiq, S., Bashir, S., Riaz, S., Naseem, S., Soleimani, H., & Yahya, N. (2016). Pulsed laser deposition of SmCo thin films for MEMS applications. *Journal of applied research and technology*, 14(5), 287-292.
- Němec, P., Frumar, M., Jedelský, J., Jelinek, M., Lančok, J., & Gregora, I. (2002). Thin amorphous chalcogenide films prepared by pulsed laser deposition. *Journal of non-crystalline solids*, 299, 1013-1017.
- Jeong, K., Park, S., Park, D., Ahn, M., Han, J., Yang, W & Cho, M. H. (2017). Evolution of crystal structures in GeTe during phase transition. *Scientific Reports*, 7(1), 955.